Novel Shape Indices for Vector Landscape Pattern Analysis

Ce Zhang

June 2015

Novel Shape Indices for Vector Landscape Pattern Analysis

by

Ce Zhang

Thesis submitted to the University of Southampton, UK, in partial fulfilment of the requirements for the degree of Master of Science in Geo-information Science and Earth Observation.

Specialisation: Environmental Modelling and Management

UNIVERSITY OF Southampton

DECLARATION OF AUTHORSHIP

I, <**Ce Zhang**>, declare that the thesis entitled "**Novel Shape Indices for Vector Landscape Pattern Analysis**" and the work presented in the thesis are both my own and have been generated by me as the result of my own scholarship. I confirm that:

- This work was done wholly while in candidature for a Masters degree at this University.
- Where any part of this thesis has previously been submitted for a degree or any other qualification at this University or any other institution, this has been clearly stated.
- Where I have consulted the published work of others accreditation has always been given.
- I have acknowledged all main sources of help.
- Where the thesis is based on work done by myself jointly with others, I have made clear exactly what was done by others and what I have contributed myself.
- It parts of this work have been published, they are listed below.

1. I have read and understood the University's Academic Integrity Statement for Students, including the information on practice to avoid given in appendix 1 of the Statement and that in this thesis I have worked within the expectations of this Statement.
http://www.calendar.soton.ac.uk/sectionIV/academic-integrity-statement.html

2. I am aware that failure to act in accordance with the Academic Integrity Statement for Students may lead to the imposition of penalties which, for the most serious cases, may include termination of programme.

3. I consent to the University copying and distributing my work and using third parties to verify whether my work contains plagiarised material. If a paper copy is also required for submission it must be identical to this electronic copy. Any discrepancies between these two copies may be considered as an act of cheating.

Signed .... Date ....

Disclaimer

This document describes work undertaken as part of a programme of study at the University of Southampton. All views and opinions expressed therein remain the sole responsibility of the author, and do not necessarily represent those of the University.

Abstract

Landscape patterns are defined as the composition and spatial arrangement of various landscape elements with different size and shape, which strongly influences the ecological processes and characteristics. Landscape pattern indices are quantitative approaches commonly used in landscape pattern analysis. Most landscape indices (including many fractal methods) are developed at landscape patch level, using a perimeter–area relationship. However, these fractal methods often fail to capture important aspects of landscape function and ecologically meaningful information, due to the ignorance of distributional differences in various directions within the patch and spatial heterogeneity between patches.

In this research, novel shape indices have been proposed to accurately describe and characterize patch orientation and shape complexity. Two geometrically invariant bounding boxes, namely, the minimum width bounding box (MWBB) and moment box (MB), were newly introduced and built up to represent patch orientation and geometric characteristics. Vector shape indices were further developed based on aforementioned boxes to reflect inner structure and shape complexity related to spatial anisotropy (geometrically oriented features), such as orientation, orientation difference between MB and MWBB, MWBB length-to-width ratio, perimeter-perimeter ratio, area-area ratio between polygon and MWBB etc.

Practical experiments have been conducted in Western Songnen Plain, Northeast China using Landsat 8 OLI imagery and ancillary data to test the effectiveness of novel shape indices. Three types of saline soils have been distinguished with spectrally similar characteristics but geometrically different. They are further classified into slightly saline soil along a large paleolake shore, moderately saline soil around current lakes and severely saline soil continuously distributed at the central region of large paleolake, based on geometric symmetry, elongatedness, compactness, etc. quantified by novel shape indices. A statistically significant increase of classification accuracy and kappa coefficient has achieved by the proposed novel shape indices in comparison with traditional shape indices, including perimeter-area ratio, fractal dimension and shape index. Finally, by linking the classification results to ecological functions, distinct differences in vegetation and soil physical properties were found in slightly, moderately and severely saline soils differentiated by the proposed novel shape indices. Therefore,

the novel shape indices are promising approaches for vector landscape pattern analysis and ecological quantitative modelling.

Acknowledgements

I would like to thank the European Union Erasmus Mundus GEM scholarship program for fully funding my studies and stay in Europe. It has been a great opportunity to improve my skills, experiences and qualifications on this course and I feel greatly indebted. The opportunity to study at ITC, University of Twente, the Netherlands and the University of Southampton, UK was life changing. I had an amazing multicultural experience.

My greatest gratitude and appreciation goes to my supervisor Professor Peter M. Atkinson for his valuable guidance, constructive feedback and comments from the very beginning till the completion of this research. Professor Pete, I owe my sincerest appreciation to all of your help, support and motivation on developing my masters research and dissertation. It is such a great honor for me to work with an excellent scientist like you and we share the common research interests in remote sensing and GIS. Your dedicated working style and scientific attitudes deeply influenced my life and world-view. I enjoyed working with you forever!

I would like to extend my gratitude to Professor Steven M. De Jong and Dr Elisabeth Addink for their comments and suggestions during my field visit at University of Utrecht, which greatly help to improve my research at the final stage of my project. I am sure we will collaborate further in the near future.

I am grateful to my Chinese advisor Professor Shuqing Zhang at Northeast Institute of Geography and Agroecology, Chinese Academic of Sciences (NEIGAE CAS). Professor Shuqing Zhang, we had lots of emails and Skype meetings to exchange ideas during my MSc research, which really inspired and helped me.

I would also thank to my advisor Dr Tiejun Wang in ITC for his unconditional support all the way back to my first foundation year study in Faculty of ITC, University of Twente. Dr Wang, You guided me how to do scientific research and contributed comments and suggestions on my first publication during my MSc study.

In addition, my thanks go to my GEM colleagues (2013 – 2015). You are all amazing people and company with me during the last 22 month, particularly our GEM group at Southampton, UK. Although some of my friends are in ITC, Lund University and Muhammad Aufaristama at University of Iceland. You are all remaining in my memory forever. My thanks also come to NRM 2013 – 2015 fellows at ITC, the PhD students at Geography and Environment department, University of Southampton, UK, particularly to Andrew MacLachlan, Sarchil Bagg, Julio Pastor Guzman, and Terry Yu.

Finally, my deepest gratitude goes to my parents for their moral supports and unconditional love during this whole period of time. You have always special place in my heart.

Table of Contents

List of figures

List of tables

1 Introduction

1.1 Background and Significances

The term landscape ecology was initially coined in 1939 by German bio-geographer Carl Troll, aimed at interpreting the relationship between vegetation and its corresponding environment. Contemporary synopsis of landscape ecology, presented by Forman and Godron (1986), and more recently by Turner (2005), emphasizes the strong influence of spatial pattern on ecological processes at a myriad of scales and organizational levels. The habitats in which certain endangered species lives, for instance, are spatially structured and heterogeneous across space at various scales, implicating the spatial distribution and flow of energy, materials and populations within a particular landscape.

Landscapes are most frequently represented by the so-called patch-corridor-matrix model, which describes the structure of a landscape as an assemblage of some dominant land-uses characterized by relatively homogenous patches, ranging from natural terrestrial and aquatic ecosystems such as forests, grasslands, and lakes to human-dominated environments including agricultural and urban settings. The particular spatial configuration of patches is crucial to characterize the landscape structure and the boundaries of patches represent the discontinuities in environmental characteristics relevant to certain species or ecological phenomenon under consideration (Turner, 1990).

Landscape patterns, or structure, are generally defined as composition and spatial configuration of phenomena over space (Turner, 1989; Bailey and Gatrell, 1995; Csillag and Kabos, 2002). The composition refers to the non-spatial measurements of landscape elements by indicating the number and occurrence of different categories. While the spatial configuration presents the physical distribution or structural arrangements at certain scales. The quantification of landscape patterns is considered as a prerequisite to the study of structure, function and reciprocal interactions between spatial pattern and ecological processes, that are fundamental pursuits of landscape ecology (Wu and Hobbs, 2007; Helfenstein et al., 2014).

Landscape patterns analysis using indices or metrics has received increasing attention in both ecological research and management communities (Cissel *et al.*, 1999; Fu and Chen, 2000; Monica G. Turner, 2005). Much efforts have been put forward on developing landscape pattern metrics, and literally hundreds of indices have been developed over the last decades (Ares et al. 2001; Honnay et al. 2003; Chust et al. 2004; Pascual-Hortal & Saura 2006; Saura & Pascual-Hortal 2007; Rizkalla et al. 2009; Llauss & Nogué 2012; Fan & Myint 2014). These indices are originated from various perspectives and disciplines, such as statistical measures of dispersion, information theory, fractal geometry and percolation theory et al (Li and Archer, 1997). In addition, new indices are still being designed (Li et al., 2005), such as aggregation index (He et al., 2000), cohesion index (Opdam et al., 2003), landscape expansion index (Liu et al., 2010). Most of these indices have been incorporated into several software packages, for example Fragstats, Patch Analyst, r.le et al. (Baker and Cai, 1992; McGarigal and Marks, 1995; O'Neill *et al.*, 1999; Kupfer, 2012).

Landscape pattern indices can describe the composition and spatial characteristics of landscape quantitatively based on GIS vector maps, aerial photographs and remotely sensed imagery. In general, three levels have been characterised for a given landscape using landscape pattern indices, i.e. the landscape patches, classes of patches and entire landscape mosaics (Uuemaa *et al.*, 2009). Ideally, the goal of landscape analyses should then be able to link measurements of landscape structure to specific effects on ecological processes, rather than treating the quantitative description of spatial pattern as an end itself. However, Li and Wu (2004) identified a number of issues related to the use and misuse of landscape indices, including misunderstanding of ecological relevance, improper utilization of indices and challenges in interpreting landscape indices.

Landscape patches with relatively homogenous configurations represent the basic but essential properties of landscape pattern at certain scales (Wu, 2004). Heterogeneity of environmental conditions, processes and interventions lead to various patches with different sizes, shapes, types and boundaries. Geometric shape of landscape patches may be an important factor in characterizing biodiversity, stability and functionality (Li, 2000). As a primary characteristic, the shape and size of a patch may be the reflection of landscape elements, but they are also influenced by local factors of environment (Forman, 1995; Hamazaki, 1996; Tanner, 2003). For this reason, the analysis of landscape structure using landscape metrics permits the accumulation of knowledge on the function of patches and their possible responses to natural and anthropogenic changes.

Characterizing landscape patches and their mosaics have become possible with the advances in remote sensing and geographic information system (GIS) techniques (Liu *et al.*, 2010). Critical to the entire landscape pattern analysis is the production of landscape land cover/use classification by remote sensing, which relies upon the acquisition of remotely sensed data and the identification of information extraction methodologies that are appropriate to the landscape characteristics under investigation (Groom *et al.*, 2006). Conventional pixel-based classifiers manipulate a single image element (e.g. spectral colour or tone), such as maximum likelihood, neural network, decision trees et al., often face the challenge of the so-called salt-and-pepper-effect over spectrally mixed and heterogeneous landscape. Object-based image analysis (OBIA) has been proposed as an alternative to the pixel-based classification approaches, that acts as a bridge between the increasing amounts of geospatial data and complex feature extraction problems (Blaschke and Strobl, 2001; Benz *et al.*, 2004; Blaschke, 2010; Puissant *et al.*, 2014). It involves segmenting images into homogeneous regions and characterizing objects with a set of features related to spectral, spatial and contextual properties (Mathieu *et al.*, 2007; Moskal *et al.*, 2011; Vieira *et al.*, 2012). Those geographic objects are essentially represented as landscape patches with relatively homogenous and distinctive properties, which might be linked to the ecological function and human perception under a particular scale.

Geometric shape is an important parameter in modelling the processes of human vision and perception (Belongie *et al.*, 2002; van der Werff and van der Meer, 2008; Vieira *et al.*, 2012). Apart from commonly used spectral characteristics for identifying objects, the shape can provide unique information for feature extraction. For example, some of the building footprints may present similar spectral colours but with different geometric shape and functions, which could be used as residential, commercial or industrial urban fabric. In addition, certain object exhibits unique shape but with different spectral properties. For instance, river meanders can be fully water filled, be filled in by sediment, be overgrown by vegetation, or a combination of these three land cover situations might occur. However, the shape of the meander will remain unchanged, thus offering a unique property that can be used to identify meanders independent from their land cover appearance (Addink and Kleinhans, 2008; Blaschke *et al.*, 2014).

Modelling the shape of an object, however, might be complicated without unified definitions and hardly to be measured directly. Therefore, shape analysis in OBIA often relies on indices that describes the shape complexity, i.e. whether they tend to be simple and compact, or irregular and convoluted. The geometric feature indices in OBIA emphasize particular aspects of geometric shape, primarily include ellipticity and rectangularity, which are commonly available in commercial software, such as ecognition. Yet, those shape indices developed in ecognition often approximated as ellipse or rectangular by estimating the pixel distribution within an object.

Such elliptic fit or rectangular fit could indirectly represent the patch properties. For example, how much close is the object to a standard ellipse and the flatness of objects are estimated by the flattening of an ellipse. Similarly, the main direction of object is approximated by the major axis of ellipse. These geometric fittings might be able to represent the geometry into numerical numbers, but the shape could be completely different and hardly be able to reconstruct the original shape by these fitted numbers. In other words, the object would better to be the same as or at least similar to ellipse in order to achieve the accurate approximation. This prerequisite might be satisfied in certain applications, especially in non-spatial domain such as human facial pattern recognition, medical imaging et al.

1.2 Problem Statement

The needs for quantitative landscape modelling and analysis using landscape pattern indices (LPIs) have been emphasised in the literature over the last three decades by O'Neill *et al.* (1988), Turner (1989, 1990, 2005), Pickett and Cadenasso (1995), Gustafson (1998), Wu and Hobbs (2007). Most indices are developed based on geometric properties of landscape elements and describe shape complexity using simple quantitative measurements (Lausch and Herzog, 2002). However, Some LPIs provide ambiguous information about spatial patterns with similar values describing several different landscapes. Typical shape indices are based on perimeter-area relationships like perimeter-area ratio, fractal dimension and shape index et al. They are dimensional metrics and involved various uncertainties in describing shape that are liable to be direction dependent, i.e. spatial anisotropy. Vector analysis theory for landscape pattern (VATLP) was initially introduced by Zhang *et al.* (2006), marked the beginning of vector landscape pattern analysis for theoretical analysing the landscape patterns with vector orientation. Object-based image analysis (OBIA) has been proposed as a method to derive tangible, GIS-ready objects from remotely sensed images by addressing complex feature recognition problems. However, no research has been done on object-based vector landscape pattern analysis to characterise shape complexity related to spatial anisotropy. The purpose of this research is to develop a series of novel shape indices that can adapt to spatial anisotropy and link to distinctive ecological functions.

The effectiveness of the method will be demonstrated by modelling and characterizing different kinds of saline soils in western Songnen Plain, Northeast China. The expert in paleogeography and soil scientist working in Da'an Sodic land experiment station provided the

reference maps about the different degree of salinity within the study area. They found that the slightly saline soils are mostly aggregated along a large paleolake shore, the moderately saline soils are generally clustered around current lakes, and the severely saline soils are mainly concentrated continuously at the central region of the large paleolake. However, the geographic and spatial distributions of different degree of salinity are not commonly available. It is therefore urgently demanded to build a detailed saline soil spatial database, in order to make spatial decision support on scientific saline soil management.
Different types of saline soils have similar spectral properties, thus hardly being distinguished based on remote sensing spectrum. However, patches of different saline soil types demonstrate distinct geometric characteristics, such as orientation, elongation, circular shape, etc. It is therefore especially useful to develop geometric quantitative methods to capture these geometric properties, so as to carry out accurately saline soil landscape pattern analysis.

1.3 Research Objectives

- To develop novel shape indices that can adapt to spatial anisotropy.
- To test the effectiveness of the novel indices on characterizing different kinds of saline soils which are geometrically different, but spectrally similar.
- To link the saline soil classification to ecological function level based on vegetation and soil physical properties.

1.4 Research Problems

1. How should novel vector landscape indices be developed to theoretically analyse patch geometric shape?
2. Can the novel shape indices be successfully applied to differentiate saline soils between elongated, circular and irregular features?
3. Is there a statistically significant difference in accuracy for classifying different kinds of saline soil between proposed novel shape indices and traditional shape indices?
4. Can the saline soil classification be linked to ecological functions?

1.5 Research Approach

The conceptual framework of this research is shown in Figure 1, in which four major blocks have been closely connected. The research starts by developing a series of novel shape indices that consider orientation, symmetry and shape complexity simultaneously. These novel shape indices are thereafter applied to vector landscape pattern analysis, with typical experiment of saline soil classification to differentiate between elongated, circular and irregular features. The effectiveness and separability of the indices have been investigated in feature characterization and modelling. In addition, the classification has been compared with traditional shape indices, including perimeter-area ratio, fractal dimension and shape index, to test the effectiveness and robustness of newly developed approach. Finally, preliminary analysis has been conducted on linking the different saline soils measured by vegetation and soil physical properties to further validate ecological meaning of the classification results.

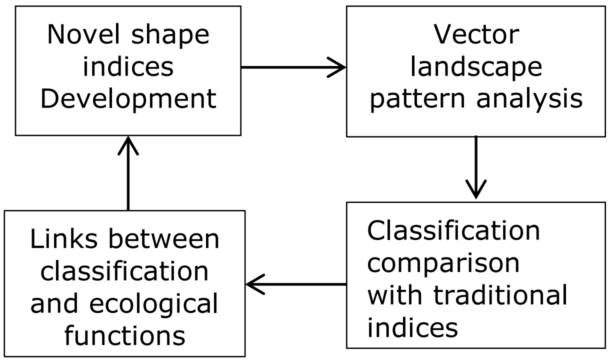

Figure 1 The conceptual diagram of approaches in the research.

2 Literature Review

2.1 Traditional geometric shape indices

Traditional geometric shape indices commonly used in landscape pattern analysis are based on the relative amount of perimeter per area to measure the complexity, usually presented as a perimeter-to-area ratio, or as a fractal dimension, and often normalized to a simple Euclidean geometry (e.g., circle or square) (Moser *et al.*, 2002). Such fractal analysis by perimeter-area relationships are originated from the scientific milestone of fractal geometry and fractal dimension by Mandelbrot in 1983 (Mandelbrot, 1983), which extends the usual ideals of classical Euclidean geometry in regard to point, segments and circle towards wider range of fractal geometry such as irregular, disjoint and singular features et al (Li, 2000). Many existing literatures elaborated on the concept of fractality from different perspectives, reaching an agreement on geometric shape with self-similar characteristics under different scales (Leduc *et al.*, 1994; Camastra and Vinciarelli, 2002; Shen, 2002; Bruno *et al.*, 2008). Fractal dimension is a quantitative measurement of complexity of the shape, depending to the irregularity, self-similarity and scale dependency of the corresponding objects (Piasecki, 2000).

Theoretical fractal objects, such as Mandelbrot set, are self-similar, meaning that any small pieces of the objects are roughly similar to the whole. But these types of fractals are rarely used to approximate objects or shapes from the real world (Shen, 2002). And therefore, the other types of fractal are suitable to describe real-world objects with self-affine. These fractals are actually self-similar as well, but through affine transformation, like translation, rotation, scaling et al. Such phenomenon is closely related to scale invariant, indicating that the same characteristics can be observed at different scales. The typical example of such natural objects is land cover/land use and their dynamics (Bruno *et al.*, 2008).

Fractal dimension is the quantitative measurement of shape complexity at different scales with non-integer values ranging from 1 to 2 (Li, 2000). The larger the fractal dimension value, the more complex the shape of the object presents. In terms of Euclidean geometry, dimension 1 represents as straight line, 2 as circle or square on 2-dimensional surface. While fractal theory claimed that regions with regular and less complex shape has lower fractal dimension (approaching to 1) and vice versa - the more irregular and complex shapes, the higher fractal dimension (approaching to 2).

Because of its simplicity and sound mathematical foundation, the fractal dimension has gained great popularity in spatial pattern

analysis, especially in the field of natural and geo-spatial science where the measurements of geographic objects are essential. Li (2000) comprehensively reviewed the concept and applications of fractal geometry in description and analysis of patch patterns and dynamics. A case study on fractal analysis of southern Texas savannah landscape has been conducted by him and concluded that the fractal can represent the spatial patterns and patch dynamics to some extent which requires further investigation.
Based on the traditional perimeter-area fractal analysis, landscape pattern analysis has developed a series of indices for presenting the patch shape complexity, including Perimeter-Area Ratio, fractal dimension, Perimeter-Area Fractal Dimension, shape index, et al. Nevertheless, the problems of these fractal dimension related indices are relatively insensitive to the differences in patch morphology and often present the uncertainty in patch shape identification and deformation extrapolation (Zhang *et al.*, 2006). Particularly, many patches possess significantly different shapes but may have identical values for the perimeters and areas or the perimeter-area ratio, thus resulting into the ambiguity for shape characterization using perimeter-area relationships. In addition, those indices are mainly computed in raster format in landscape pattern analysis using commercial software, such as Fragstats 4.2. The perimeter lengths are biased upward in raster images due to the stair-stepping pattern of line segments, and the magnitude of this bias varies in accordance to the grain or resolution of the images. Therefore, it is of significance to develop vector-based landscape pattern analysis that can precisely characterize and quantify the patch geometric shape.

2.2 Anisotropy in Landscape Ecology

Natural phenomenon often presents the properties of heterogeneity and anisotropy. Spatial heterogeneity in landscape ecology often results in habitat fragmentation and variation within- and between-habitat qualities (Ye *et al.*, 2013). Previous researches have shown the spatial variation in habitat patches have strong effects on population density and extinction events (Lambrechts *et al.*, 2004; Johnson *et al.*, 2005; Girvetz and Greco, 2007). On the contrary, the spatial anisotropy and corresponding ecological consequences have received little attention in landscape ecological research.
Spatial anisotropy, as opposed to isotropy, represents the directional property of spatial pattern, in which a landscape patch trends towards a certain direction or orientation. Many ecological data are produced by geophysical and environmental processes (Gustafson, 1998; Wu *et al.*, 2000). For example, the fractures, folds, and ridges on mountainous surface might be the result of tectonic activities. The ecological succession of forest ecosystem could be directional

dependent because of fire, precipitation or other climate conditions. Although anisotropic processes are arguably more common than isotropic ones, they have been received less attention in literatures because they are more problematic mathematically and requires more data for statistical inference (Waller and Gotway, 2004).
Anisotropic semivariogram modelling is the most commonly used approach for understanding the directional spatial pattern and process. Semivariogram (Second-order variogram) modelling using kriging is the fundamental tool of geostatistical analysis. The theoretical semivariogram models are built upon isotropic models, thus many researches have adapted anisotropy to the experimental semivariogram (Schönfisch, 1997). Geometrically anisotropic spatial process, for instance, has been modelled by Bayesian analysis with parameters controlling geometric anisotropy and applied successfully on digital elevation model (DEM) (Ecker and Gelfand, 1999). Besides, the existence of a directional component and the quantification of anisotropy in digital images have been conducted by (Molina and Feito, 2002). In addition, the spatial variability of sea surface temperature in the global ocean have been analysed by anisotropic semivariogram model using AVHRR data (Tandeo et al., 2014). They all conclude that the anisotropic semivariogram model using geostatistical method can reveal certain anisotropic behaviour under appropriate parameter setting. However, the experimental semivariogram has to be fitted by visual examination in different directions on global and local levels, and the large numbers of parameters involved in the model make the parameter optimization unmanageable. Thus, the necessity of developing novel analytic methods and precise quantification of spatial anisotropy in landscape ecological research is beyond doubt.

2.3 Vector analysis theory on landscape pattern

Vector analysis theory on landscape pattern (VATLP) was initially proposed by (Zhang et al., 2006). The principle of vector analysis theory has been originated from the classic mechanics. The planar properties of geometry defined in mechanics such as centroid, moment of inertia, product of inertia and principle axes are crucial since these theoretical characteristics of landscape patches help the understanding of shape and orientation, which directly link to landscape anisotropy. Based on the moments of inertia about x-axes and y-axes, the indices of patch orientation (PO) and vectorized patch orientation (VPO) can be derived from the anti-clockwise angle between the major principle axis and the horizontal line. Thereby, the patch orientation and the positive direction of patch orientation have

been extracted by (Zhang et al., 2006). In addition, the index of eccentric rate (ER) has been developed based on elliptic fit. Those indices have been successfully applied on understanding the ecological processes, such as energy and material flows, underlying the formation of ecological gradients and patterns in the Qian'an group lakes.
The idea of vector analysis theory bridged the gap between modern landscape ecology and spatial analytic geometry, and revolutionized the landscape ecological researches to link the landscape anisotropy to various ecological functions. However, the fundamental of such vector analysis theory proposed by (Zhang et al., 2006) is built upon the ellipsoidal fit and the principle axes of fitted ellipse are assumed to be exactly the same as the orientation of patch. Such elliptic approximation is rather a strong assumption and might not be sensitive enough to reflect some irregular patch shapes, due to the lack of understanding on the shape complexity related to spatial anisotropy.

2.4 Minimum Bounding Box and its application

The Minimum bounding rectangular, also known as 2-dimensional minimum bounding box, lies at the heart of many computational geometry applications, such as ray tracing, collision avoidance, and hidden object detection (Anderson and Cychosz, 1990; Hubbard, 1995; Szegedy *et al.*, 2013). The most commonly used minimum bounding box was calculated by envelope, which also named as minimum bounding envelope (Chan and Tan, 2001). The minimum bounding envelope contains the entire points in a region in the Cartesian coordinate system (Freeman and Shapira, 1975). Based on the maximum and minimum coordinates in x- and y- axis, the minimum bounding envelope can be swiftly built up and served as the simple location and representation of certain objects. This kind of bounding box has been extensively used in geographic information systems (GIS), especially in geospatial data representation and Spatial indexing schemes (Zhu *et al.*, 2007). The minimum bounding envelope covering the extent of data within a spatial dataset indicates where the geographical phenomenon occurs, and is the most useful tool for understanding whether or not the data overlaps a specific area of interest. Most geospatial standards, including ISO 19115 and Dublin Core Metadata Initiative (DCMI), present the bounding box of datasets in metadata information (Albrecht, 1999).
However, the minimum bounding envelope does not take the orientation into account, which largely restricts the applications in

computer graphics and image processing. Most geometric features computed from segmented images including elongatedness, rectangularity, moments, and other shape descriptors cannot be derived from objects themselves. The minimum bounding rectangular is considered as the essential step towards geometric feature extraction and image object understanding (Chaudhuri and Samal, 2007). Finding a minimum bounding box that can cover exactly the polygon and represent the polygon characteristics properly needs appropriate approaches.

The most widely used approach for finding the minimum bounding box was initially developed by Toussaint (1983), which was called oriented minimum bounding boxes (OMBB) in computer graphics. The idea was trying to pack convex polygons into a rectangle of smallest size, measured either by area or by perimeter. Therefore, the first step is to compute the convex hull of the input polygon using mathematical algorithms, such as Quick Hull, Gift Wrapping, Graham's Algorithm and so on. Thereafter, the so-called "Rotating Callipers" has been implemented for finding the OMBB. The assumption is that each convex hull edge should coincide with one of the four calliper lines, and the resulting OMBB is the OMBB candidate with the smallest area (Freeman and Shapira, 1975). The advantage of this method is simple and computational efficient since both steps are linear in terms of computing complexity. However, the problems of such rotating calliper approach become evident when the numbers of vertices of the input polygon are large and complex with self-intersect and holes.

More recently, Werman and Keren (2001) presents a Bayesian method for fitting the models to find both parametric and non-parametric rectangles. Saha et al. (2012) have presented a region-based approach to the fitting of objects by rectangles. These advanced approaches often require normalization of shape into unit disk and tuning of parameter settings, which are often data and application specific and largely restricted for further applications.

In (Chaudhuri and Samal, 2007), a fast method for fitting of bounding rectangle to polygon has been adopted, in which the bounding rectangle has been built upon the boundary vertices of polygon and the orientation was determined by the major axis and minor axis of the object based on centroid and moments. Such moment based minimum bounding box is promising due to its invariant to translation, rotation and scaling. However, in some situations, the boxes are not minimum and sensitive to noise and variation in the polygon vertices.

Though the minimum bounding box has been built up in various methods and widely applied in computational geometric, computer graphics and image processing et al. To the best of our knowledge, however, no research has been done on landscape pattern analysis to model the vector landscape patterns accurately. In this research, therefore, a simple but novel method has been put forward to accurately characterize the bounding box of landscape patches. It was based on a least square regression method to fit the box orientation, and the global coordinate was then transformed into the local coordinate of that regression line. The candidate oriented minimum bounding box has been constructed by the minimum and maximum coordinate. Thereafter, the minimum width has been searched by rotating certain amount of angle to ensure the box fit the polygon find the best orientation.

Based on constructed minimum width bounding box (MWBB), a series of indices could be extracted. These indices are mainly related to the orientation and shape complexity. For example, the direction and orientation of MWBB that represent the polygon global direction and orientation. At the same time, the orientation of moment box (MB) built from centroid and moment of inertia can also be obtained. The orientation difference between MWBB and MB might be useful for analysing the inner symmetric structure and indicating the potential oriented shapes. The shape complexity such as compactness can be built up by the area-to-area ratio between polygon and MWBB, the length to width of the polygon represented by MWBB, and perimeter-to-perimeter ratio can be extracted as well. These newly developed shape indices are expected to reflect the shape complexity directly related to the spatial anisotropy, which can overcome the limitations of shape characterization using traditional shape indices, such as perimeter-area ratio, fractal dimension and shape index, etc. The novel shape indices was tested on a real problem of modelling and characterizing different kinds of saline soils that are geometrically different, but spectrally similar, and further linked to their ecological functions.

3 Methods

3.1 Minimum Width Bounding Box

Minimum bounding box, in computational geometry, generally referred to the smallest enclosing rectangle with the least measure (area, width, length or perimeter) over two-dimensional space (Chaudhuri and Samal, 2007). The properties of a minimum bounding box are translation, rotation and reflection invariant in terms of its enclosing polygon, thus indicating the corresponding orientation of original polygon.
Vector landscape indices in this study are based on the minimum bounding box by width in consideration of its capability to capture the orientation of polygon. The length perpendicular to the minimum width of bounding box has been determined aligned with the oriented axis of the polygon. Although the minimum area bounding box also indicates orientation with minimum area rectangle, however, it is hardly to guarantee the length since the minimum width has not been searched. Comparisons between minimum area bounding box (MABB) and minimum bounding width box (MWBB) with a typical object are shown in Figure 2. It shows that the MABB does not have any orientations with almost horizontal of 178.9, whereas the object is actually having 148.3 degree orientation quantified by MWBB.

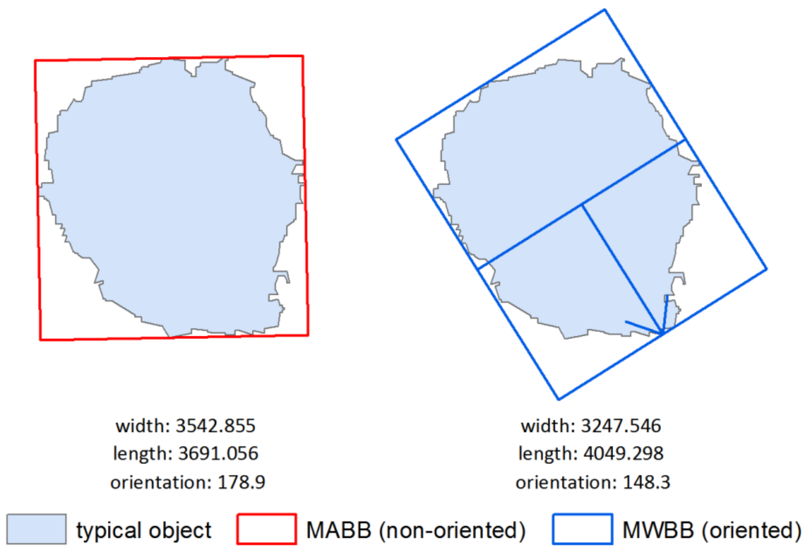

Figure 2 Comparison between minimum area bounding box (MABB) and minimum width bounding box (MWBB).

The constructions of the minimum width bounding box in this research are largely depending on the spatial distribution of the vertices along the boundary of the polygon. A least square linear regression has been conducted to fit a line, followed by an axis transformation to the local coordinate systems. The bounding box can then be built up based on the maximum projections of each vertex on the new axis. Since the vertex density and spatial distribution often influences the size of the bounding box, which is not the minimum width bounding box in most cases, the MWBB has been searched numerically by the so-called "rotation calliper" method given user defined threshold. Detailed steps for building the MWBB has been summarised below:

Step 1: Least square approximation to fit a line (Figure 3)
Linear function minimizing squared errors can be calculated as:

$$\mathrm{f(x)} = b_0 + b_1 x \tag{1}$$

2 regression parameters can be computed as (Equation 2-3):

$$\mathrm{b_1} = \frac{\sum \mathrm{xy} - \mathrm{n}\bar{\mathrm{x}}\bar{\mathrm{y}}}{\sum \mathrm{x}^2 - \mathrm{n}(\bar{\mathrm{x}})^2} \tag{2}$$

$$\mathrm{b_0} = \bar{\mathrm{y}} - \mathrm{b_1}\bar{\mathrm{x}} \tag{3}$$

Where

$$\bar{\mathrm{x}} = \frac{1}{\mathrm{n}}\sum_{\mathrm{i}=1}^{\mathrm{n}} \mathrm{x_i} \tag{4}$$

$$\bar{\mathrm{y}} = \frac{1}{\mathrm{n}}\sum_{\mathrm{i}=1}^{\mathrm{n}} \mathrm{y_i} \tag{5}$$

$$\sum \mathrm{xy} = \sum_{\mathrm{i}=1}^{\mathrm{n}} \mathrm{x_i y_i} \tag{6}$$

$$\sum \mathrm{x}^2 = \sum_{\mathrm{i}=1}^{\mathrm{n}} (\mathrm{x_i})^2 \tag{7}$$

From Equation 1-7, the parameter b1 is the slope of the fitted line, and the variable n is the number of vertex of each polygon.

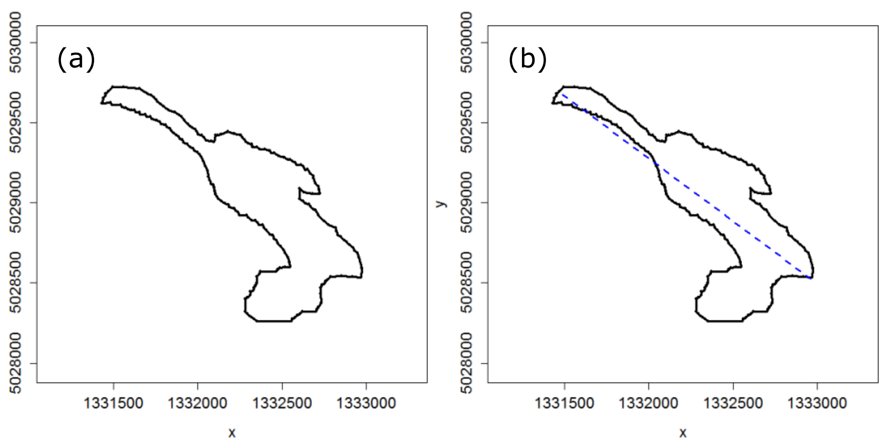

Figure 3 Illustration of linear least square approximation: (a) original polygon, (b) least square fitting by the vertices of polygon.

Step 2: Coordinate transformation based on the calculated slope
Coordinate transformation based on the fitted line (Figure 4)

$$b_1 = \tan(\theta) \tag{8}$$

$$\theta = \arctan(\theta) \tag{9}$$

Therefore, $\sin(\theta)$ and $\cos(\theta)$ can be calculated via Equation 8 and 9. Given a vertex (x, y) in global coordinate system with origin (x_0, y_0), new coordinate (x', y') can be extracted by coordinate translation and rotation (Equation 10).

$$\begin{pmatrix} x' \\ y' \end{pmatrix} = \begin{pmatrix} \cos\theta & \sin\theta \\ -\sin\theta & \cos\theta \end{pmatrix} \begin{pmatrix} x - x_0 \\ y - y_0 \end{pmatrix} + \begin{pmatrix} b_0 \cdot \cos\theta \\ b_0 \cdot \sin\theta \end{pmatrix} \tag{10}$$

By translating and rotating the axes, the x-axis in new coordinate system is along the fitted line. A point on the x-axis is randomly selected as the origin of new coordinate, and the y-axis is perpendicular to the new x-axis as shown in Figure 4.

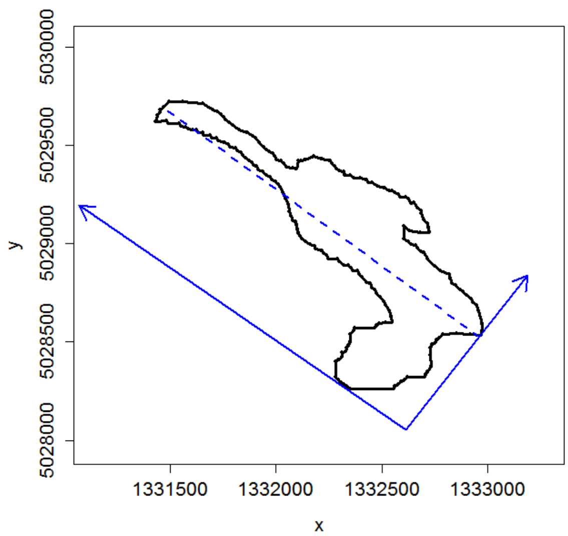

Figure 4 Illustration of coordinate transformation from original x-y coordinates into local coordinates.

Step 3: Finding the maximum and minimum coordinates of the vertices

Under the new coordinate system, the maximum and minimum y-coordinate of the vertices, Y_{min} and Y_{max}, as well as those of x-coordinate, X_{min} and X_{max}, can be determined, which then could be used as the initial minimum bounding box.

Step 4: Rotating calliper to numerically search the minimum width bounding box (Figure 5)

The main axis fitted by least square approximation is largely influenced by vertex density and distribution. Therefore, it is necessary to numerically search the best solutions for the MWBB. Both clockwise and anti-clockwise with a large scope of 40 degree has been exhaustively searched numerically. The initial angle for each rotation has been set as θ, iteratively increase or decrease a small angle (predefined as δ) to find the bounding box with minimum width or approximate to the minimum. Such bounding rectangle is minimum width bounding box (MWBB) with orientation.

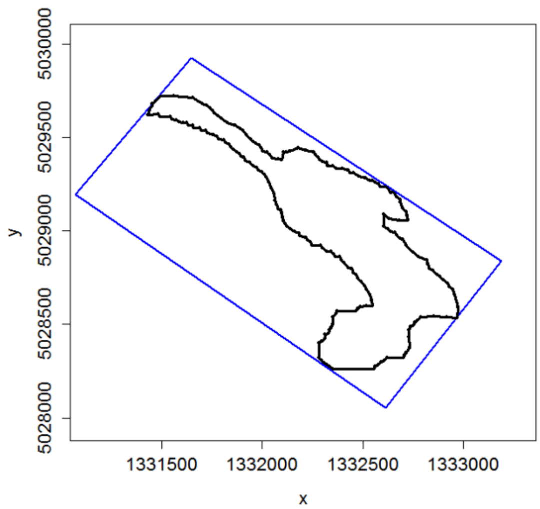

Figure 5 Patch with Minimum Width Bounding Box (MWBB).

Vector landscape indices based on Minimum bounding box

Suppose a polygon P area and perimeter as PA and PP. The area and perimeter of Minimum width bounding box are MWBA and MWBP. The length of the box is MWBL, while the width of the box is MWBW.

A series of indices can be extracted to quantify the shape complexity. These could be based on the area ratio between polygon and the MWBB, the perimeter ratio between polygon and the MWBB, minimum box length-to-width ratio.

Meanwhile, the orientation (0, 180) and direction (0, 360) of the box can be obtained. The direction is determined by the polygon area difference on different sides of the middle line of the minimum width bounding box (Figure 6). Figure 6-b shows that the upper left side of the polygon is larger than the lower right side. Thereby, the direction is toward the upper left side.

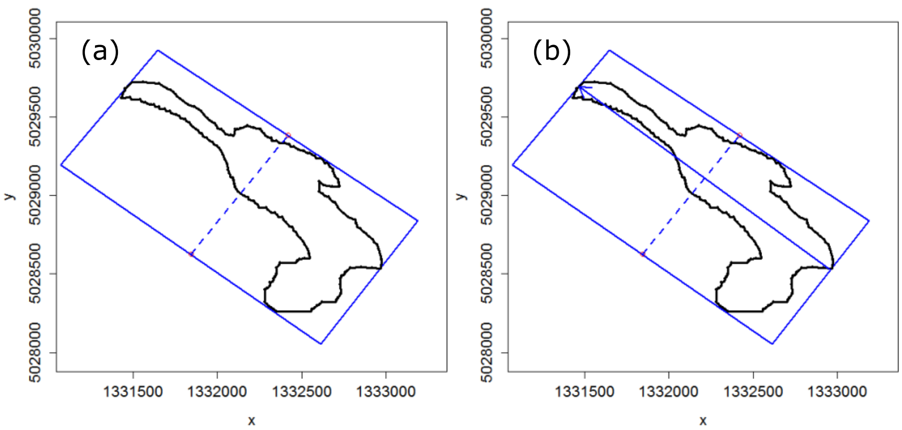

Figure 6 The determination of orientation of polygon: (a) minimum width bounding box with its middle line (b) the vector direction of the polygon derived from the differences of polygon area.

3.2 Moment Box

The moment box (MB) was built upon centroid and moment of inertia to obtain moment orientation (MO). Vector analysis theory on landscape pattern (VATLP) based on mechanics such as centroid, moment of inertia, product of inertia and principal axes was initially proposed by Zhang et al. (2006). The principle of moment orientation has been briefly reviewed as follows:

The shape of a polygon is assumed to be based on rotational motion. The moment indicates the tendency of a force to rotate an object about an axis, which is defined as the integral of the distance over entire area. Suppose (x, y) is a point within an object. The x- and y-axes are defined by the mapping coordinate system. The centroid $C(\bar{x}, \bar{y})$ can be extracted by the first order moment about x-axes (I_x) and about y-axes (I_y) (Equation 11-14). Figure 7 shows the centroid of polygon obtained by x-y coordinates.

$$I_x = \int y dA \tag{11}$$

$$I_y = \int x dA \tag{12}$$

$$\bar{x} = \frac{I_y}{A} \tag{13}$$

$$\bar{y} = \frac{I_x}{A} \tag{14}$$

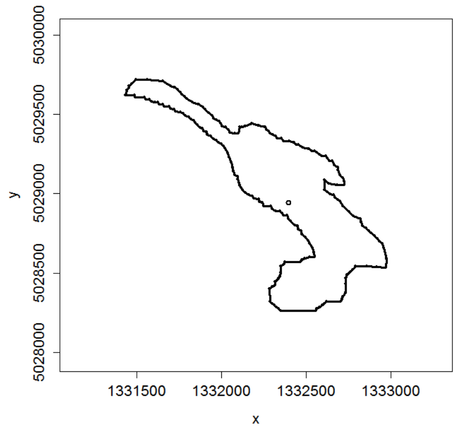

Figure 7 The centroid of polygon.

The polygon's moment of inertia determines the force needed for a desired angular acceleration about an axis of rotation. It largely depends on the shape of object and might be different between distinct axes. A larger moment of inertia requires stronger force to increase or stop the rotation. In classical mechanics, the moment of inertia about the x-axes (I_{xx}) and about y-axes (I_{yy}) as well as product of inertia (I_{xy}) can be calculated by second order moment (Equation 15-17). An illustration of Centroid and moments of inertia has been shown in Figure 8.

$$I_{xx} = \int y^2 dA \tag{15}$$

$$I_{yy} = \int x^2 dA \tag{16}$$

$$I_{xy} = \int xy dA \tag{17}$$

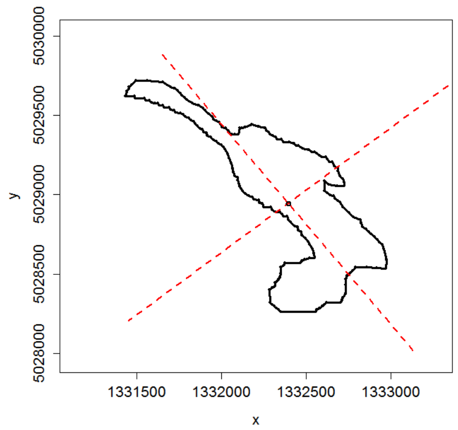

Figure 8 An illustration of centroid and moments of inertia by x-axis and y-axis.

Suppose the centroid is the origin of local coordinates. Two mutually perpendicular moments, i.e. major axis and minor axis, are passing through the centroid. The minimum rotational moment is the major axis and the maximum rotational moment is the minor axis. The moment orientation (MO) is defined as the angle between the major axis and horizontal line. The MO can be acquired by the following Equation 18-19:

$$\tan 2\theta = \frac{2I_{xy}}{I_{yy}-I_{xx}} \tag{18}$$

$$\theta = \frac{1}{2} * \tan^{-1}\frac{2I_{xy}}{I_{yy}-I_{xx}} \tag{19}$$

The above mentioned equations can be discretized to calculate the coordinates of individual vertices. Interested readers can refer to Zhang et al (2006) for the detailed equations after discretization, which are not included due to volume limitation of this dissertation.

3.3 Novel Shape Indices

All the novel shape indices are developed based on the minimum width bounding box (MWBB) and moment box (MB). These indices mainly focus on geometric orientation and shape complexity.
The orientation difference index (ODI) is an index that measures the angle between the MWBB direction and the MB major axis orientation. Figure 9 shows (a) the MWBB (blue box) and MB (red box) of polygon and (b) the angle between MWBB direction (blue line with arrow) and the MB major axis orientation (red dash line).

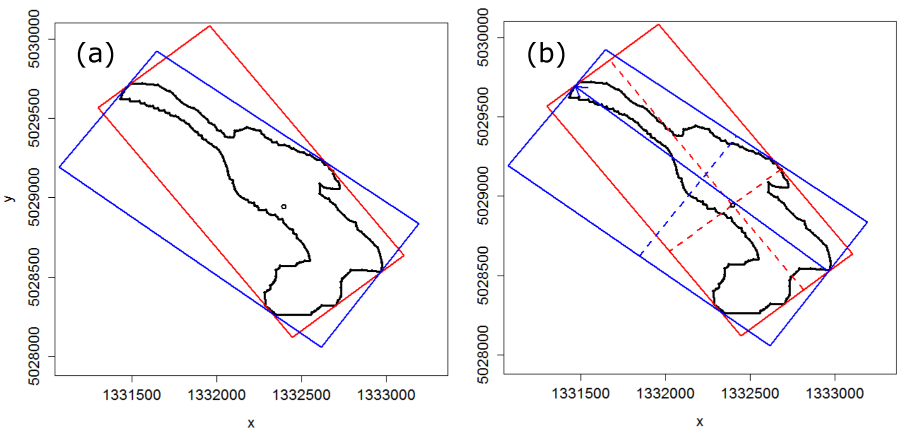

Figure 9 The orientation difference index (ODI) of polygon: (a) the combination of MWBB (blue) and MB (red) (b) the angle between MWBB direction (blue line with arrow) and the MB major axis orientation (red dash line).

The development of this ODI is to analyse the orientation of objects and indicate the inner spatial structure of geometric shape. The MWBB is considered as a benchmark of orientation and direction that does not change along with rotation, reflection and translation due to its robustness and stability in object characterization given the width of an object fixed. However, the MB is essentially built upon centroid and gravity, which is influenced by the inner shape and structural distribution. Figure 9-b shows that the bottom left corner of the red box (MB) passing through the centroid rotates downside compared with blue box (MWBB) mainly due to the extra area at the bottom left of the object. The moment orientation rotates clockwise to maintain the force balance in this case. If an object has the ellipsoid shape, then the red box and blue box will be exactly the same and the ODI will be 0. In other words, the ODI shows the characteristics of rotational symmetry properties to a certain degree. The smaller the ODI, the more symmetric the shape presents.

The shape complexity in this method is mainly related to Elongatedness (Length-to-width ratio of MWBB), Compactness (Area ratio between polygon and MWBB), ruggedness (Perimeter ratio between polygon and MWBB). These features are developed to characterize the complexity of certain objects and to recognize the emerging patterns. These features are dimensionless and robust for classification without changing along with the size of the shape, which might be able to infer certain classes of objects with distinctive geometric properties. For example, some of the objects may have the properties of elongatedness and high compactness but with low ruggedness, which represents some special patterns.

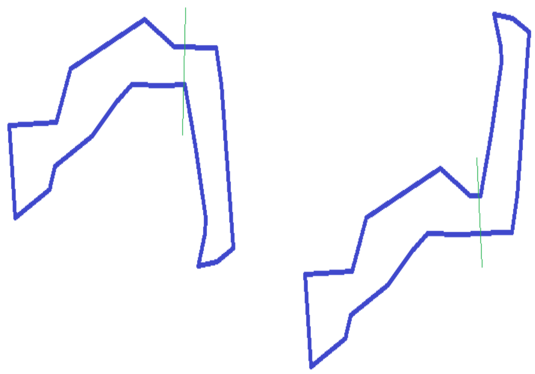

Figure 10 Same ratio of patch perimeter and patch area, shape complexities are equally measured by traditional shape metrics, but with completely different geometric shape.

These features are developed to recognize some geometric shapes that have same or similar perimeter-area ratio but completely with different shapes. Figure 10 shows a typical example of such kind of object with exactly the same perimeter-area ratio but different geometric shape because of anisotropic orientation. The patches (objects) having the same perimeter-area ratios will lead to uncertainties based on traditional shape indices related to perimeter-area relationship. By describing the orientation, elongatedness, compactness in regard to MWBB, the uncertainty of landscape modelling and pattern analysis would be reduced or even eliminated by appropriate applications.

Table 1 Detailed description of novel shape indices and traditional shape indices in this study.

Method	Indices (Acronym)	Description
Proposed Novel Shape Indices	MWBB Orientation (MO)	The orientation (0-180 **degree**) of minimum width bounding box
	MWBB Direction (MD)	The direction (0-360 **degree**) of minimum width bounding box
	MWBB Length/Width (MWBBLW)	The ratio between length (**m**) and width (**m**) of minimum width bounding box
	Polygon Area/MWBB Area (PAMWBA)	The ratio between polygon area (**m^2**) and minimum width bounding box area (**m^2**)
	Polygon Perimeter/MWBB Perimeter (PPMWBP)	The ratio between polygon perimeter (m) and minimum width bounding box perimeter (**m**)
	Orientation Difference Index (ODI)	The angle between direction of MWBB (0-360 **degree**) and Moment box major orientation (0-180 **degree**)
Traditional Shape Indices (Neel *et al.*, 2004)	Perimeter-Area ratio (PARA)	The ratio of the patch perimeter (**m**) to area (**m^2**)
	Shape index (SHAPE)	patch perimeter (**m**) divided by the square root of patch area (**m^2**), adjusted by a constant to adjust for a square standard
	Fractal Dimension (FRAC)	2 times the logarithm of patch perimeter (**m**) divided by the log of patch area (**m^2**)

Table 1 summarized the proposed novel shape indices and traditional shape indices. The description of novel shape indices presents the orientation (degree) and dimensionless shape complexity. However, the traditional shape indices including polygon perimeter-area ratio, shape index, fractal dimension, have the dimensional properties. The dimensionless characteristics of the proposed novel shape indices can potentially overcome the uncertainties of shape characterization resulting from the variation of patch size.

4 Study Area and Data Material

4.1 Study Area

The study area is located between 122°03′41′′E – 124°38′45′′E and 43°54′58′′N – 45°45′50′′N, the hinterland of western Songnen Plain, Northeast China, mainly covering western Jilin Province and Inner Mongolia Autonomous Region (Figure 11). The climate of this area is characterized as temperate continental monsoon ranging from semi-humid to semi-arid with an annual average temperature of 4°C (Chi and Wang, 2010). Monthly temperature in January is from -16°C to -26°C and that in July is from 21°C to 23°C. The frost-free period is about 151 days each year from late May to early November (Dianwei *et al.*, 2009).

Annual mean precipitation is around 370-400 mm with 80% falls in July and August, causing a moisture deficit during 7 months per year (Wang *et al.*, 2009). But the annual evaporation reaches to 1700-1900 mm in average. So the evaporation 4-5 times greater than the precipitation. Seasons alternate between dry and windy springs, humid and warm summers with intensive rainfall, windy and dry early-frost autumns and long, severe cold winters with relatively little snowfall.

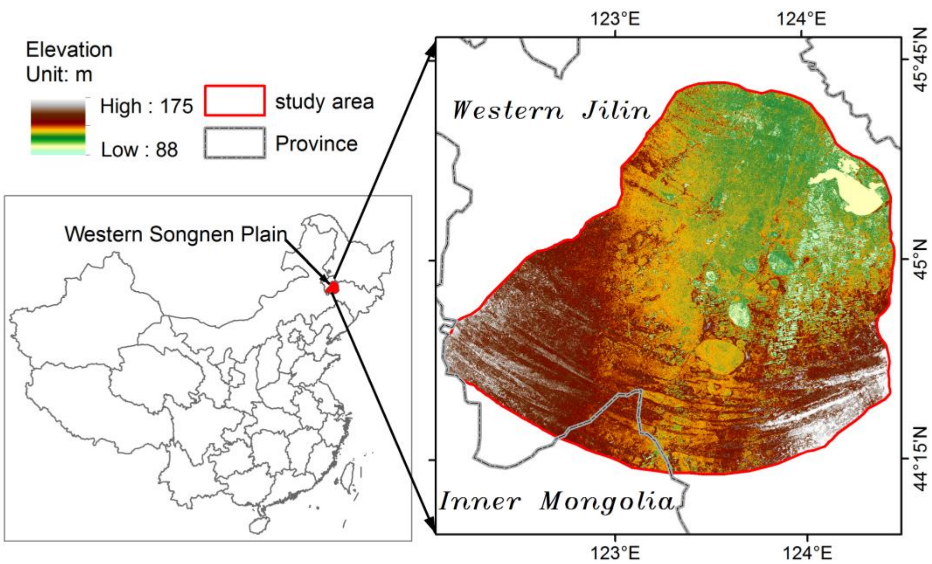

Figure 11 Map of the study area delineated in red polygon. The image presented is DEM elevation within study area.

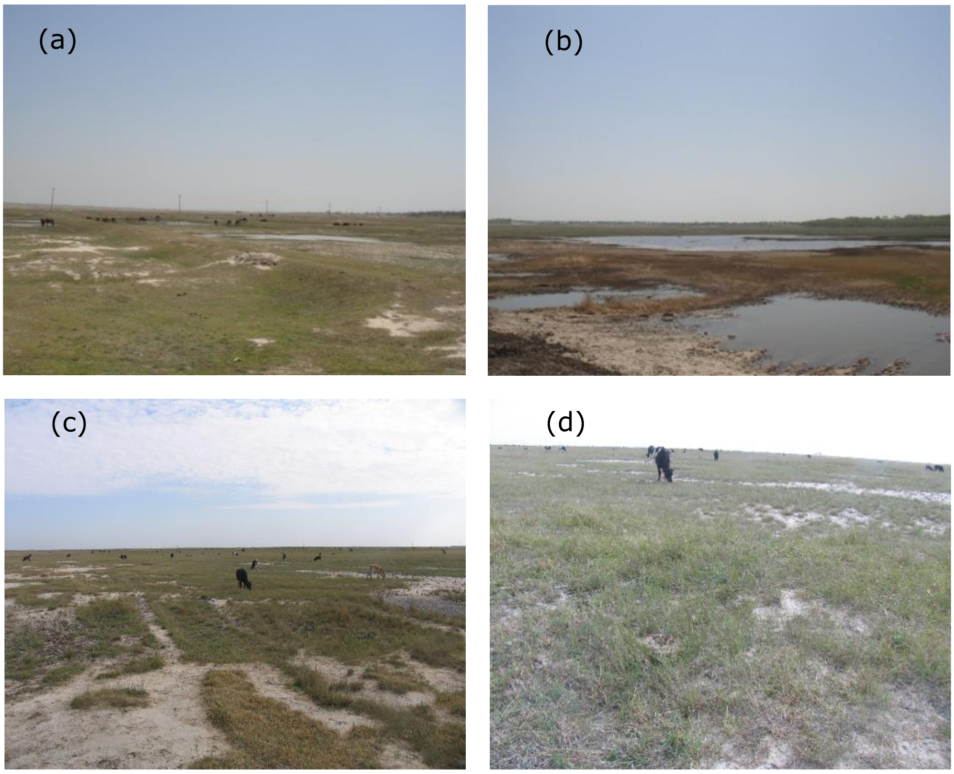

Figure 12 Example photos of the saline soil characteristics of Western Songnen Plain, Northeast China during September: (a) slightly saline soil along large paleolake shore, (b) moderately saline soil around current lake, and (c, d) severely saline soil at central region of the large paleolake.

The soil salinization and alkalization of western Songnen Plain has been widely concerned as a major environmental problem related to land degradation and reduced rangeland productivity. Figure 12 shows the photos of typical saline soil at western Songnen Plain with clear white colours, which requires careful attention as a major impediment to sustainable agriculture. The development of these salt-affected soils is a comprehensive result of several natural environmental factors, including climate, geology, parent material, hydrological conditions, water chemistry, and the freeze-thaw factor. The study area was located within a large paleolake, the so-called Songliao Paleolake, formed after the Triassic Era by seawater incursion events due to tectonic and geological activities (Hu *et al.*, 2015). The total area of the large paleolake was about 5×10^4 km^2 and the geographic extent of such paleolake was roughly illustrated by (Qiu *et al.*, 2012) according to the sedimentary sequences and

lithological characteristics of more than 500 bores. The paleolake gradually disappeared at the beginning of Late Pleistocene due to the slow rise of the Songnen Plain and long term dry cold climate, left some elongated patterns of saline soils along the large paleolake shore formed by some complicated geomorphological processes over a long period of time. At the central region of the large paleolake, the western Songnen Plain had deposited over 5000 meters alluvial-lacustrine sediments and had been separated into numerous salt-affected lakes. Those lakes and surrounding saline soils are primarily moderately saline soil according to reference maps created by local experts. These moderately saline soils are highly oriented landscape influenced by the strong prevailing wind in winter from northwest to southeast, as the extreme dry weather condition and sandy, uncovered soil characteristics. In addition, the soil freeze-and thaw processes have given rise to upward movement and evapo-concentration of soluble salts present in shallow groundwater (Zhang and Shijie, 2001). The surface evaporation and low soil permeability have resulted in the severely saline soil continuously distributed with high degree of salt accumulation. However, those saline soils along the large paleolake shore mostly have low degree of salinity, in regard to the relatively high elevation of local topography and shallow ground water tables.
Due to soil salinization, no natural tree species exist in the study area. The western Songnen Plain is extremely ecological fragile and lack of biodiversity. Only some of the salt tolerant grass communities can grow on these salt-affected soils, such as *Leymus chinensis*, *Puccinellia tenuiflora* and *Suaeda corniculata*.

4.2 Data Material

4.2.1 Landsat 8 OLI Imagery

Three cloud-free scenes acquired by the Landsat 8 OLI imagery captured on 15 September 2014 (Path 120, Row 28-29 and Path 119 Row 29) were used in this research. The images were composed of seven multi-spectral bands (Coastal, Blue, Green, Red, NIR, SWIR1 and SWIR2) with a spatial resolution of 30 m.
The atmospheric effects of the imageries were removed using 6S atmospheric radiative transfer model by accurately converting the measured at-sensor radiance to surface reflectance (Vermote et al., 1997). The images were then geo-rectified to the Transverse Mercator Projection based on a topographic map at a scale of 1:50 000 using 50 evenly distributed ground control points. A third order polynomial model was used for rectification implementing the nearest neighbour algorithm with a pixel size of 30 m × 30 m for all bands.

The root mean square errors were less than 0.5 pixels (15 m). Finally, a mosaic was constructed by these three scenes covering the entire study area.

4.2.2 Ancillary Data

The ancillary data used in this study include: 1) the National Land cover/Land use Database of China, 2) Reference maps of different saline soil types provided by local experts, 3) Obview-3 Panchromatic images and other high resolution imageries 4) geophysical data of the study area, 5) vegetation atlas of China.

1) National Land cover/Land use Database of China (NLUCD-2000) was used as a reference land cover data for assisting image segmentation and initial accuracy assessment. It was visually interpreted from remotely sensed images on 21 September 2000 (Landsat TM 30 m × 30 m), and stored in ArcGIS Geodatabase. The interpretation was based on "The Standard of Remote Sensing Interpretation of Land Resource Investigation of China" (Liu *et al.*, 2002; Boles *et al.*, 2004). The overall accuracy of classification is over 85%. For more detailed information about the interpretation, please see (Liu *et al.*, 2003)and (Xian *et al.*, 2009).

2) Reference maps of saline soil types have been provided by the local experts, including the expert in paleogeography and soil scientists working in Da'an Sodic land experiment station. They found that different degrees of salinity within the study area are strongly correlated to specific geographic location and geometric shape. Most of the slightly saline soils are along a large paleolake shore, the moderately saline soils are generally clustered around current lakes, and the severely saline soils are mainly concentrated continuously at the central region of the large paleolake. These reference maps are used as expert knowledge to develop rule sets for feature extraction.

3) Obview-3 Panchromatic images and other high spatial resolution imageries were used as object-based signature training and accuracy assessment. The Obview-3 Panchromatic images were downloaded from EarthExplorer of U.S. Geological Survey (USGS) (http://earthexplorer.usgs.gov). Other Quickbird and Worldview-2 images were acquired from Bing Map Aerial (©2013 Nokia, ©2014 Microsoft Corporation) and Google Maps (Image © 2014 CNES / Astrium, Google Map data ©2014). The training and validation sample plots were carefully selected by visual interpretation for object-based vector pattern analysis.

4) The geophysical data involved in this study includes Digital Elevation Model (DEM) and geomorphological map of Northeast China. The ASTER Global Digital Elevation Model (ASTER GDEM) was collected in October 2011 using stereo-pair images generated by ASTER sensor at ground resolution of 30m. The geomorphological

map was used as assistant reference for micro-relief on a scale of 1 ：100 000 (Committee of Geomorphological Map of China, 2009). Both of them were reprojected to Transverse Mercator Projection and then subset to the study area.

5) The Vegetation Atlas of China was used to guide the interpretation and link the classification to the ecological function. It is worth mentioning that the Vegetation Atlas of China is currently the most detailed material in reflecting vegetation types and their distribution across China. It includes 54 vegetation types and 796 vegetation communities and sub-communities (Huang and Siegert, 2006). In order to facilitate the utility of the Vegetation Atlas of China, under the support of projects "Environmental & Ecological Science Data Centre for West China, National Natural Science Foundation of China" (http://westdc.westgis.ac.cn) and "Data-sharing Network of Earth System Science", totally 60 maps covering all of China were digitized by Cold and Arid Regions Environmental and Engineering Research Institute, Chinese Academy of Sciences (Ran *et al.*, 2012). The digital maps were then matched and spliced, and each digital boundary was assigned to a lot of vegetation attributes including vegetation type, vegetation community and sub-community. In this research, the digital vegetation atlas was overlaid with the classified objects in geographical information system (GIS) environment to link the saline soil class to vegetation communities and ecological functions.

5 Results and analysis

5.1 Spectral Segmentation and Object-based Classification

5.1.1 Spectral segmentation

The initial step for object-based image analysis is image segmentation. The multi-resolution segmentation algorithm was carried out in eCognition 8.9 software. Multi-resolution segmentation is a bottom-up region-merging approach based on the idea of Fractal Net Evolution (Baatz and Schape, 2000; Benz *et al.*, 2004). The objects were grouped into meaningful information according to geographic features based on scale and homogeneity parameters. The homogeneity parameters are further determined by the parameters of shape and compactness. The interested objects in this research are saline soils and lakes, particularly saline soils with complex geometric shape highly influenced by spatial anisotropy. These features are rather spectrally distinctive and compact. On remote sensing image, the saline soils present brilliant white colour and the lakes are pure blue or dark blue, and most of them are clustering into certain locations. Therefore, we set the shape parameter as 0.2 (0.8 for spectral) and the compactness to be 0.8.

The determination of appropriate scale in OBIA is very challenging (Drăguţ *et al.*, 2014). The degree of heterogeneity within an image object is controlled by a scale parameter by a subjective measure. In eCognition Developer 8.9 software it is called scale parameter. The average size of segmented image influences on the accuracy of classification. Thus, the decision of scale parameter selection is essential in remote sensing segmentation.

The ESP (Estimation of Scale Parameter) tool was used to estimate the appropriate scales built on the local variance of object heterogeneity within a scene (Woodcock and Strahler, 1987; Drăguţ *et al.*, 2010). Figure 13 shows the rate of change and local variance estimated by ESP tool in the study area. The optimal scale of OBIA is 85 with a peak of ROC (0.72).

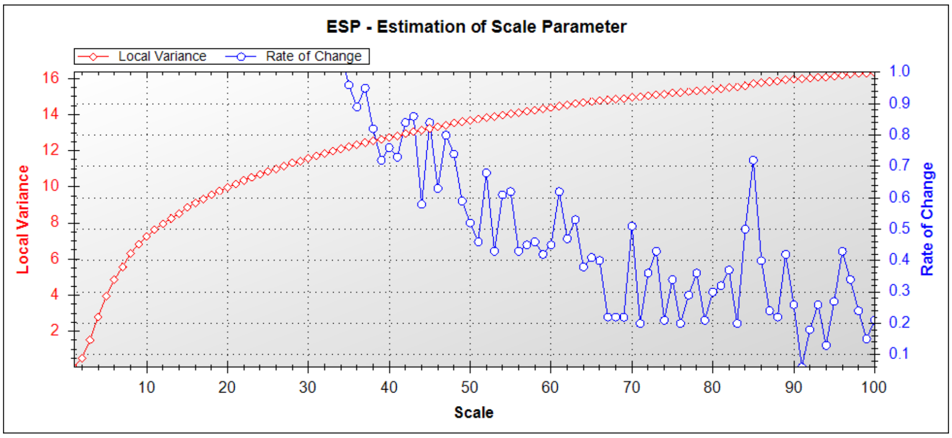

Figure 13 Optimal scale size estimated by ESP (Estimation of Scale Parameter) tool with optimal scale parameter: 85 (ROC: 0.72).

The multi-resolution segmentation was implemented with a scale parameter of 85. The partial view result was shown below in Figure 14(a), in which most of the interested objects are over-segmented. For example, the lake has been segmented into different parts. Therefore, the spectral difference has been used to reduce the meaningless over-segmentation. The maximum spectral difference has been parameterized by trial-and-error and determined as 40 in this study. Figure 14(b) illustrates the effects of combining multi-resolution segmentation and spectral difference segmentation. The objects of interest (saline soils and lakes) have been maintained without much confusion visually.

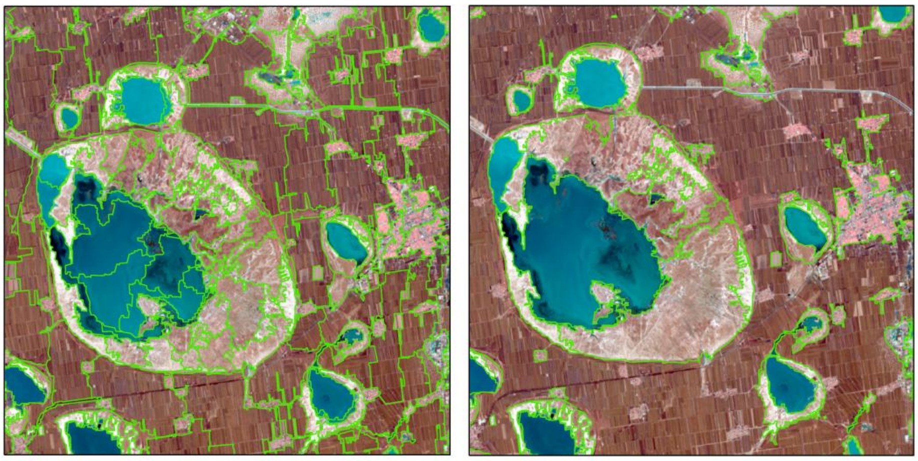

Multi-resolution Segmentation

Multi-resolution Segmentation
Spectral Difference Segmentation

Figure 14 The comparison between multi-resolution segmentation and multi-resolution segmentation combined with spectral difference segmentation.

Segmentation problems still maintain visually in terms of over-segmentation and under-segmentation. Particularly, some of the artificial objects like roads and bridges break the entire objects into different parts (over-segmentation). Meanwhile, some of the villages and rivers are highly close to the saline soils or lakes, which wrongly mix them together as an object (under-segmentation). Therefore, the segmentation was further improved by two experts in OBIA through manual rectification. The final segmentation results are illustrated by Figure 15.

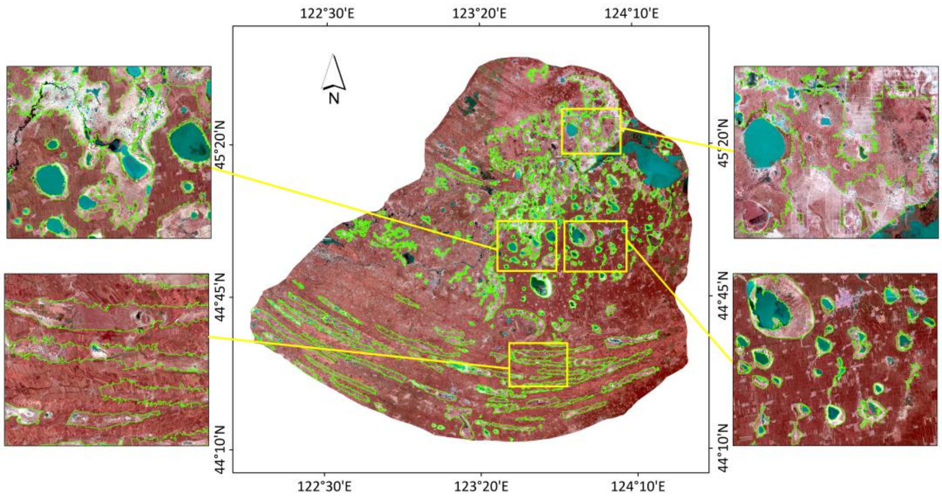

Figure 15 The final segmentation results in the study area.

5.1.2 Object-based classification

The object-based classification was based on the spectral brightness of Landsat 8 OLI (7 bands) assisted by the thematic information of National Land cover/Land use Database of China (NLUCD-2000) using object-based nearest neighbour classifier. The training sample sets of saline soils, lakes and others have been selected all over the study area and the classification results were shown in Figure 16. The overall classification accuracy was higher than 85% by visual cross validation with Obview-3 Panchromatic imagery downloaded from USGS (Earth explorer), Bing Map Aerial and Google Maps.

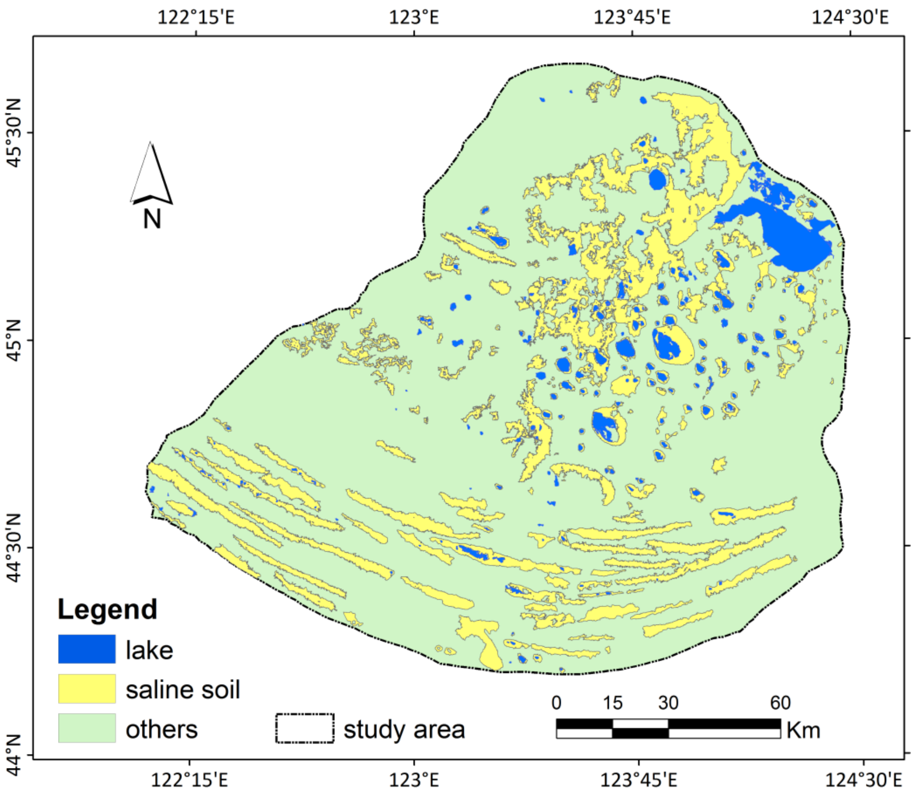

Figure 16 Object-based classification results of lake and saline soil.

5.2 Spectral Separability of Saline Soil

Known from local experts in geography and paleoecology, the saline soils in the study area are generally fell into three different types, i.e. slightly saline soil along a large paleolake shore, moderately saline soil around current lake and severely saline soil continuously distributed at the central region of the large paleolake. The three kinds of saline soils are complex features with distinct geometric shape. Before further investigating the geometric shape, however, spectral information is commonly used to differentiate different degree of salinity, especially with traditional pixel-based classification approach. Therefore, it is necessary to test the spectral separability among these three types to identify whether they are separable in spectral tone.

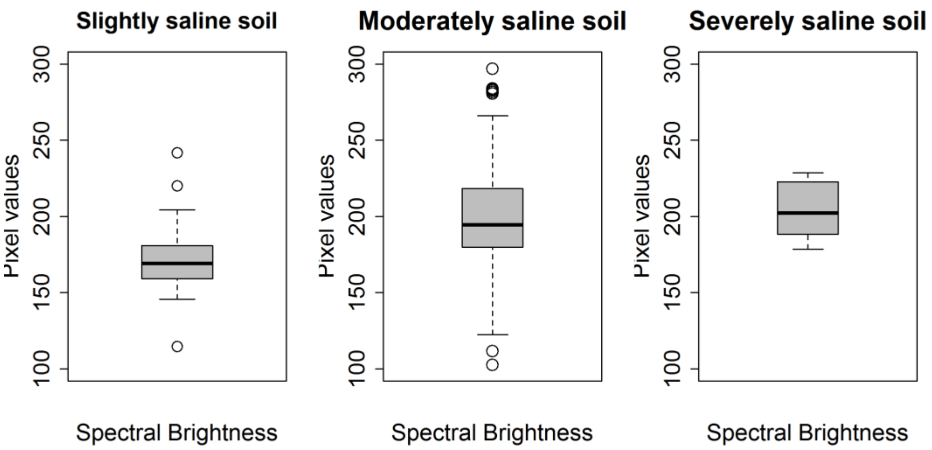

Figure 17 The spectral brightness comparison among three different saline soil types, i.e. the slightly, moderately and severely saline soil.

Figure 17 shows the boxplot of spectral brightness among three different kinds of saline soil. The slightly saline soils along large paleolake shore are slightly smaller than those moderately saline soil around current lake, but still has some overlaps in terms of spectral brightness. While the spectral brightness of moderately saline soil is mostly the same as that of severely saline soil. The variabilities of moderately saline soils are high with large standard deviation and some outliers in comparison with other two types of saline soils.
Each band comparison between three different types have been shown in Figure 18, which further proves our findings in spectral separability.

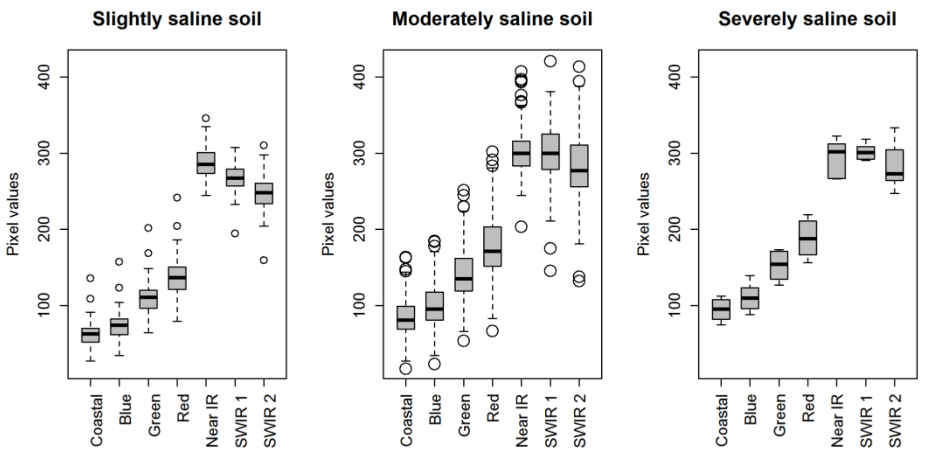

Figure 18 Each band of Landsat 8 OIL comparison among three different saline soil types, i.e. the slightly, moderately and severely saline soil.

5.3 Saline Soil Pattern Extraction

5.3.1 Slightly Saline Soil Shape Extraction

Object-based vector landscape pattern analysis has been carried out by rule-based feature extraction. The slightly saline soil has been identified by orientation, elongatedness and compactness. The detailed rule sets are given in Table 2.

Table 2 Detailed rule sets developed for feature extraction of slightly saline soil.

Shape descriptor	Shape indices	Rules
orientation	Orientation difference index	<= 4.6
Elongatedness	Minimum width bounding box length/width	> 3
Compactness	Area ratio between polygon and minimum box	> 0.34

The feature extraction result of the slightly saline soil (45 patches) has been shown in Figure 19.

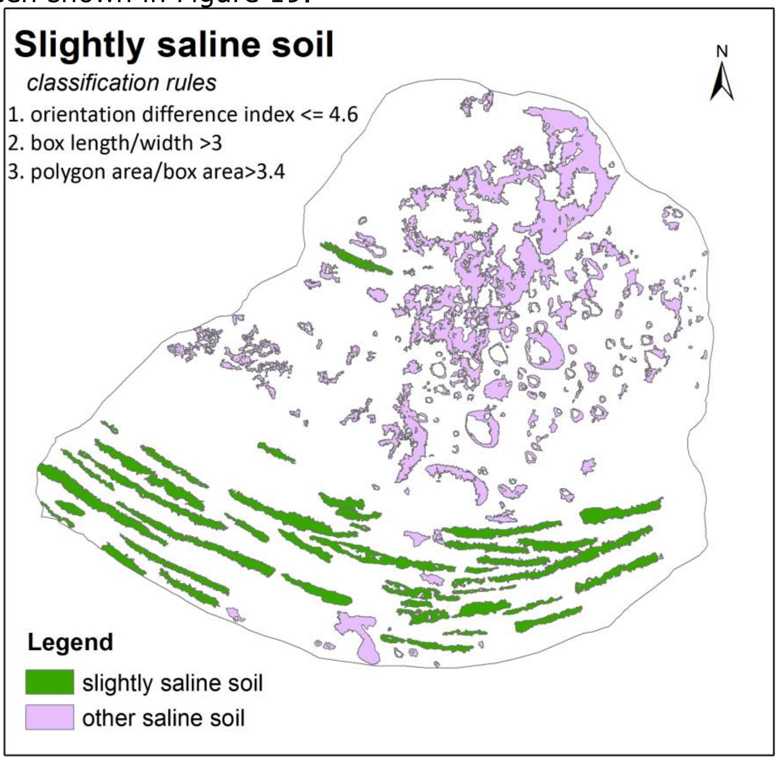

Figure 19 The feature extraction of the slightly saline soil.

1) Orientation Feature Extraction

"Orientation difference index" has been built up based on the characteristics of paleolake shore (strongly oriented) with relatively small orientation difference between minimum width bounding boxes and moment boxes. The orientation difference is a relative measurement showing the orientation and symmetric information. The smaller orientation difference indicates the higher level of orientation and symmetric properties. The threshold of orientation difference has been set less than 4.6 to extract the relative small orientation difference. Figure 20 illustrates the results of orientation extraction.

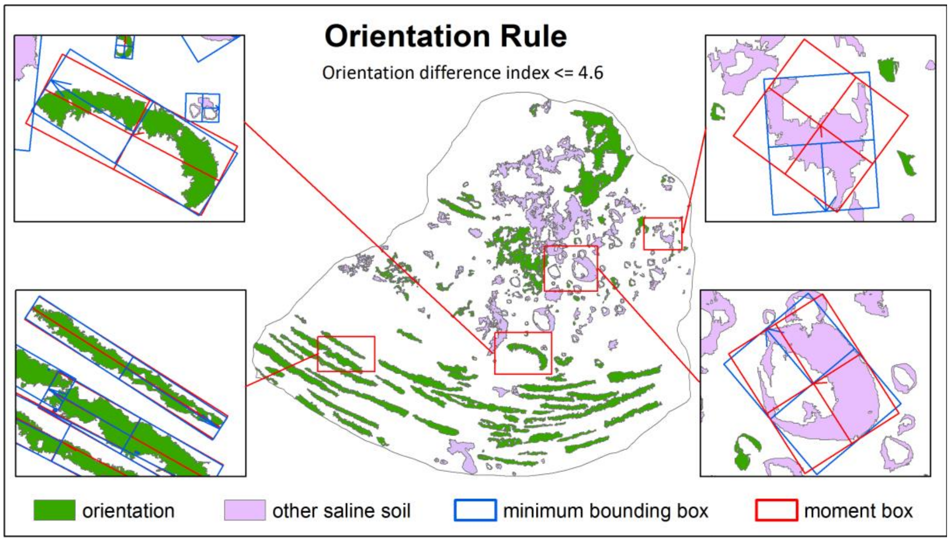

Figure 20 The illustration of orientation difference index (ODI) rule sets developed for orientation feature extraction of slightly saline soil.

105 out of 225 patches have been extracted by the orientation rule sets. From Figure 20, the slightly saline soils have been maintained.

2) Elongatedness Feature Extraction

The shape of the slightly saline soils can also be described by elongatedness because of the elongating shape. The minimum width bounding box length/width has been threshold larger than 3 to extract elongatedness features. The 105 patches have been dramatically reduced to 47 patches by elongatedness, which has been shown in Figure 21.

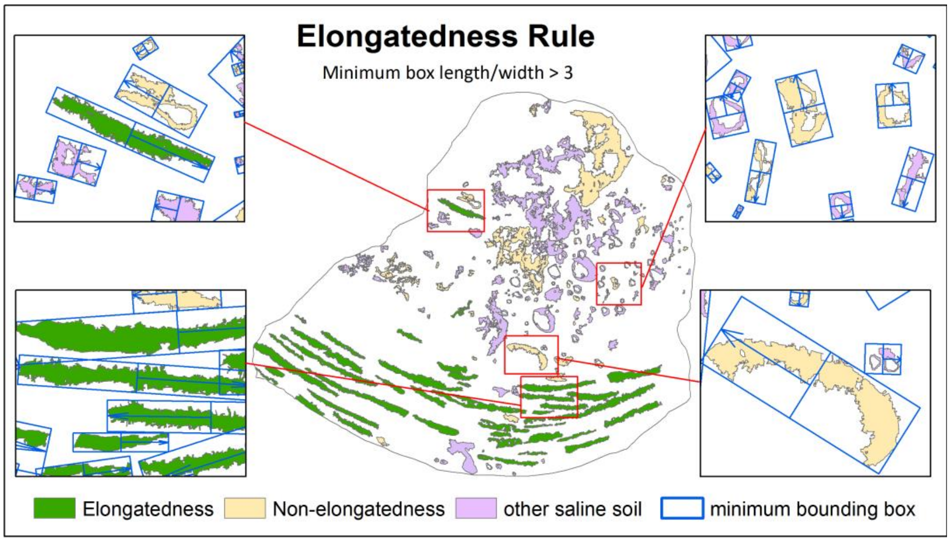

Figure 21 The illustration of minimum box length/width rule sets developed for elongatedness feature extraction of slightly saline soil.

3) Compactness Feature Extraction

The slightly saline soils are generally compact. The area ratio between polygon and minimum box has been set larger than 0.34 to obtain the high compactness. Two more patches have been removed because of low compactness, with compactness value of 0.328 and 0.315 respectively. The results of these two objects and other 45 remained patches have been highlighted in Figure 22.

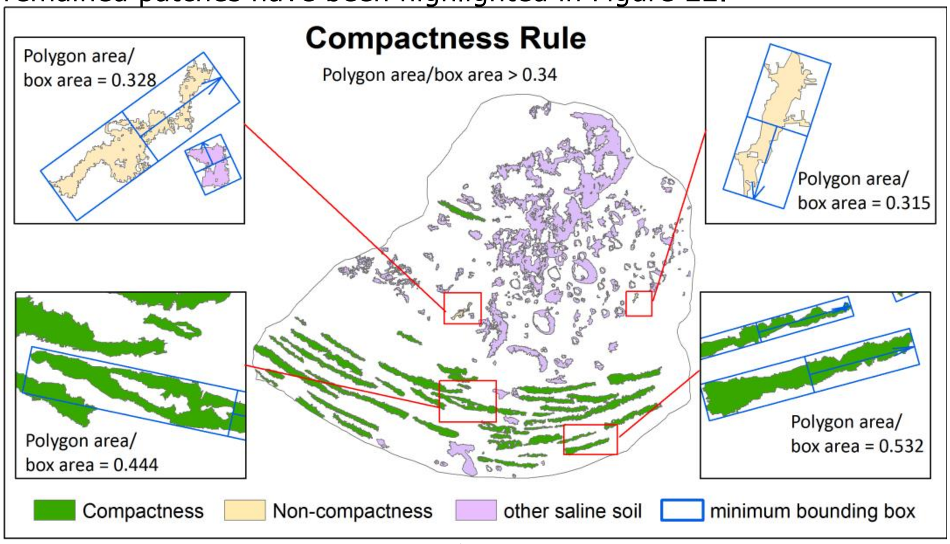

Figure 22 The illustration of polygon area/box area rule sets developed for compactness feature extraction of slightly saline soil.

5.3.2 Moderately Saline Soil Shape Extraction

The moderately saline soil has been extracted by its complex circular shape. The length-to-width ratio (minimum bounding box length to width), compactness (area ratio between polygon and MWBB) as well ruggedness (perimeter ratio between polygon and MWBB) have been used to describe the shape characteristics of moderately saline soil. Table 3 shows the rule sets of moderately saline soil classification.

Table 3 Detailed rule sets developed for feature extraction of moderately saline soil.

Shape descriptor	Shape indices	Rules
Length-to-width ratio	Minimum width bounding box length/width	< 2.8
Compactness	Area ratio between polygon and minimum box	(0.18 - 0.57)
Ruggedness	Perimeter ratio between polygon and minimum box	< 2.22

The classification results of moderately saline soils have been shown in Figure 23, in which 117 patches have been extracted out of 225 patches.

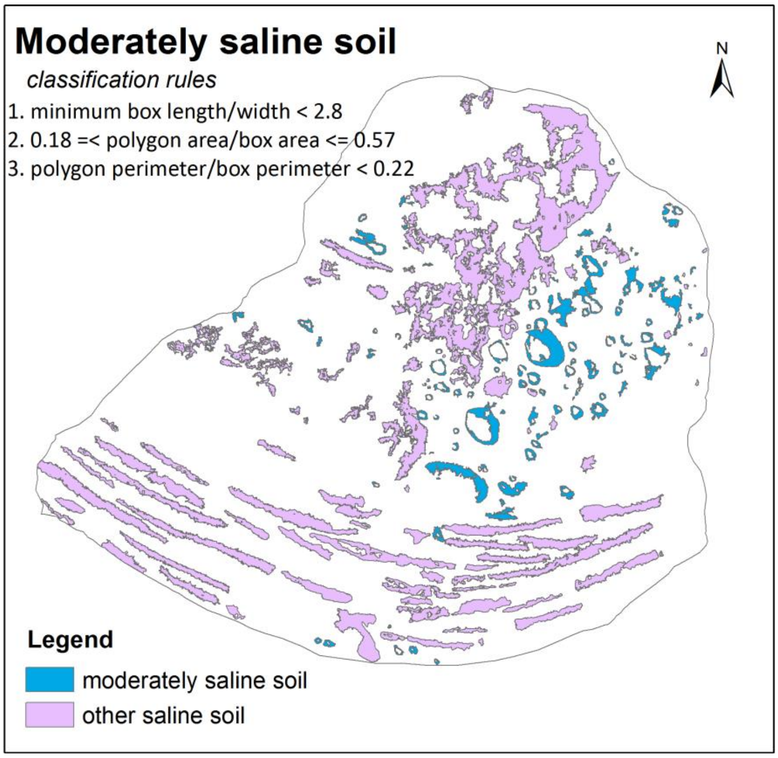

Figure 23 The feature extraction of the moderately saline soil.

1) Length-to-width ratio feature extraction

The length-to-width ratio (minimum bounding box length to width ratio) of moderately saline soils is low because most of the saline soils around current lakes are tend to be circular shape with similar length and width. In this research, the length-to-width ratio has been tuned to less than 2.8 to obtain relatively small aspect ratio. The classification results of length-to-width ratio with 172 patches out of 225 have been shown in Figure 24.

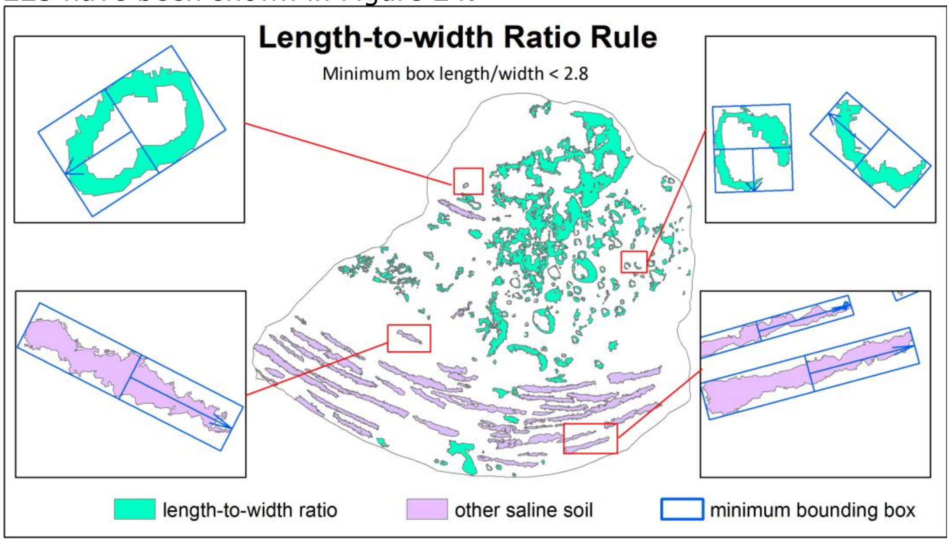

Figure 24 The illustration of minimum box length/width rule sets developed for compactness feature extraction of moderately saline soil.

2) Compactness feature extraction

Most of the moderately saline soils are crescent-shaped circular and curved elongating shapes surrounding the current lakes, with relatively low compactness. The threshold of area ratio between polygon and box has been set larger than 0.17 and smaller than 0.51 to get the relatively small compactness. The resulting compactness of moderately saline soil has reduced to 128 patches from 172 patches previously (Figure 25).

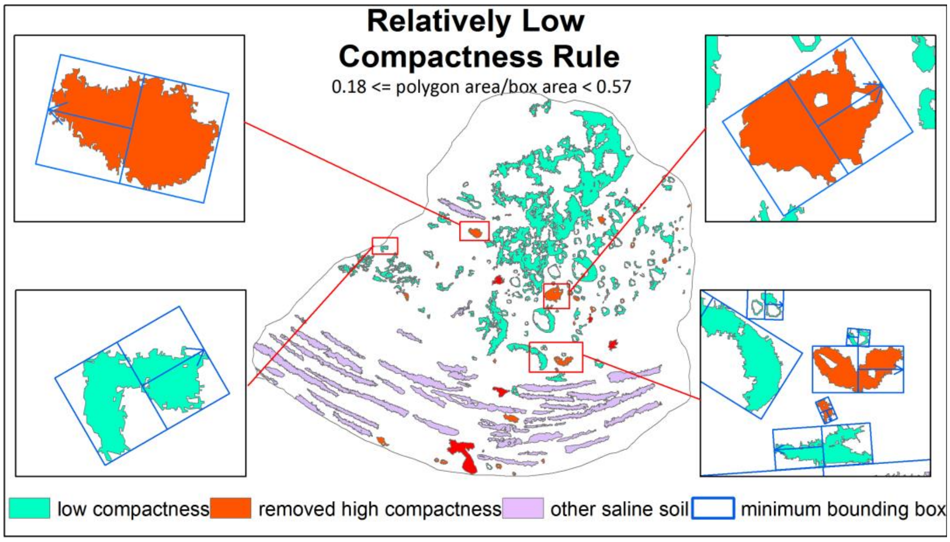

Figure 25 The illustration of polygon area/box area rule sets developed for relatively low compactness feature extraction of moderately saline soil.

3) Ruggedness feature extraction

The shapes of moderately saline soil are mostly low boundary roughness in comparison with severely saline soil and close to circle in a certain degree. The ruggedness is described by the perimeter ratio between polygon and box, which is set to be smaller than 2.22 to remove the complex rugged shapes, which the final 117 lake saline soils have been extracted. Figure 26 shows the results of classification with highlight of the removed shape that has high ruggedness.

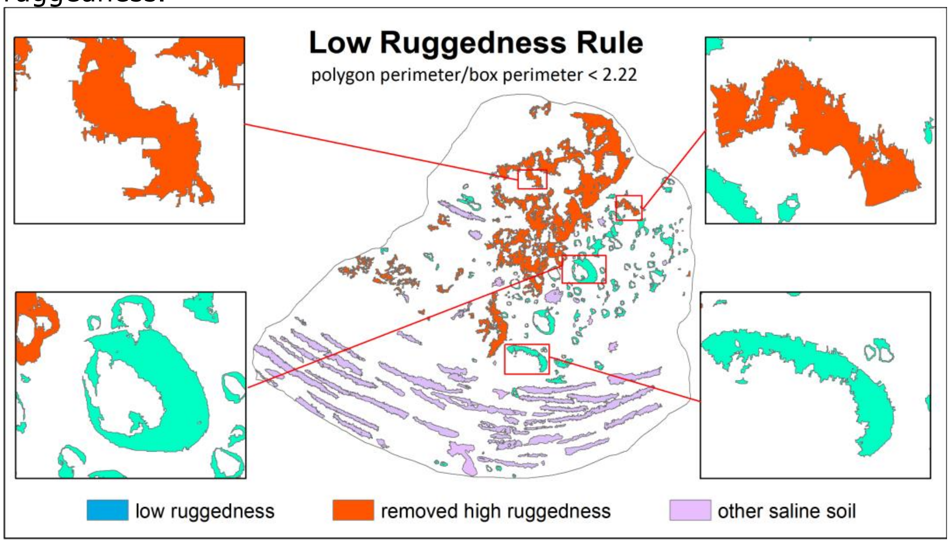

Figure 26 The illustration of polygon perimeter/box perimeter rule sets developed for low ruggedness feature extraction of moderately saline soil.

5.3.3 Severely Saline Soil Shape Extraction

The extraction of severely saline soil is purely built upon size and geometric shape. The developed rule sets are based on large polygon area and high ruggedness (high perimeter ratio between polygon and box). These two classification rules can directly extract the 9 patches of severely saline soil. The detailed rule sets and classification results have been shown in Table 4 and Figure 27 respectively.

Table 4 Detailed rule sets developed for feature extraction of severely saline soil.

Shape descriptor	Shape indices	Rules
Area	Polygon area	>= 14400000
Ruggedness	Perimeter ratio between polygon and minimum box	> 3.4

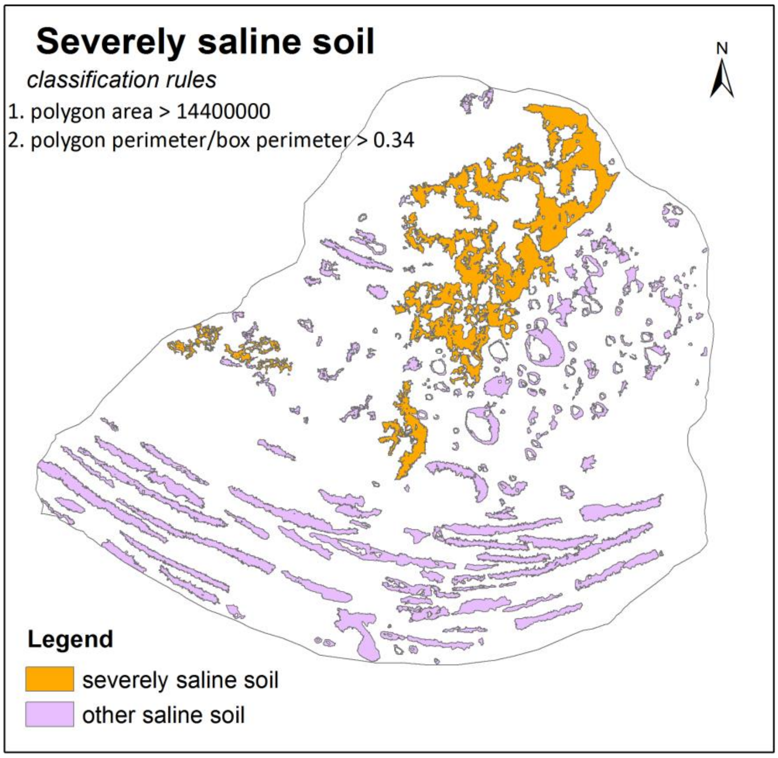

Figure 27 The feature extraction of the severely saline soil.

5.3.4 Saline Soil Classification Results

The final classification results have been shown in Figure 28. Four kinds of saline soils have been identified, i.e. slightly saline soil, moderately saline soil, severely saline soil and other saline soils. Note, the other saline soils are the features with uncertain shapes scattering around villages, farmland, et al.

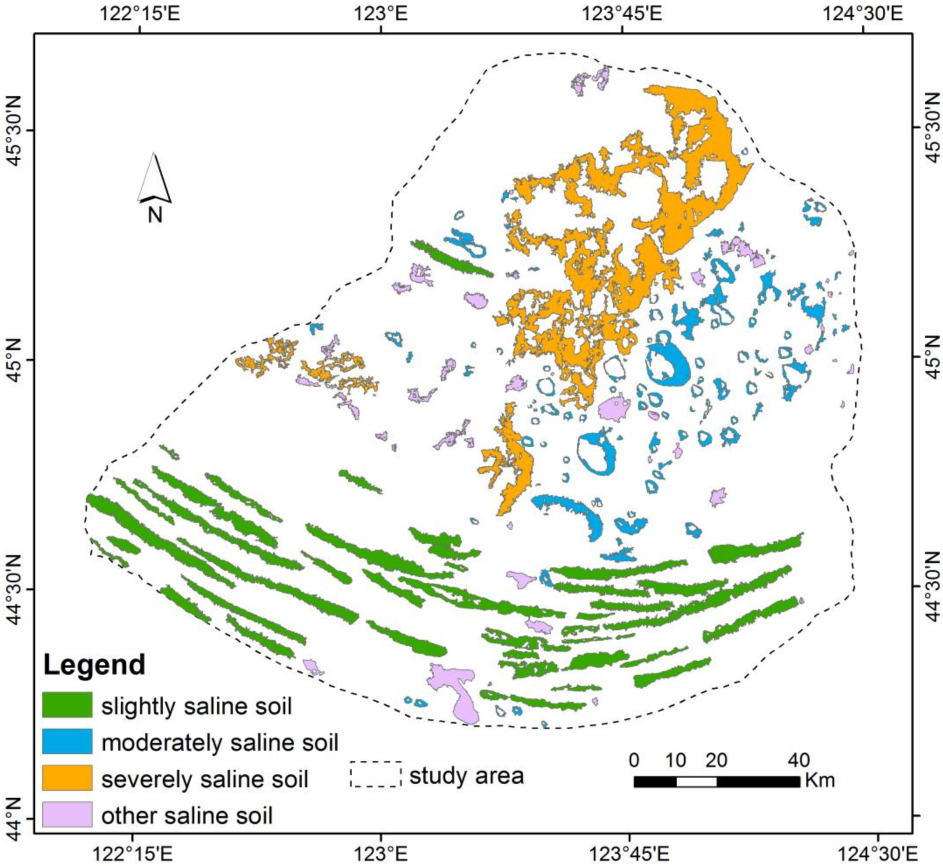

Figure 28 The final saline soil classification results.

5.4 Spatial Statistics of Three Saline Soils

5.4.1 Basic Statistics of Slightly Saline Soil

The basic statistics of slightly saline soil have been summarized by Table 5. It involves statistical elements of each feature, which is minimum, maximum, mean and standard deviation (SD). The preliminary features calculated by the vector landscape pattern analysis include area, perimeter, area ratio between polygon and box (PA/BA), perimeter ratio between polygon and box (PP/BP), orientation difference index (ODI), length to width ratio (MWBL/MWBW), box orientation. Detailed information of 45 patches of slightly saline soils has been presented in Table 5.

Table 5 The basic statistics (Minimum, Maximum, Mean and Stand Dev.) of novel shape indices for slightly saline soil

Slightly saline soil (45)	Area	Perimeter	PA/BA	PP/BP	ODI(°)	MWBL/MWBW	Orientation (°)
Minimum	3984300	16015	0.35	0.953	0.017	3.11	0.042
Maximum	104804370	239558	0.603	3.044	4.53	18.358	179.895
Mean	39260409	112316	0.477	2.147	1.12	6.163	120.027
Stand Dev.	25806153	60273	0.069	0.399	1.026	3.068	68.382

The orientation histogram has been shown in Figure 29. Most of the orientations are within 0-30 degree or 140-180 degree (0 and 180 degree are equally horizontal). The slightly saline soils within study area mostly locate at the southern part of the large paleolake shore, with the distribution of East-West oriented fan. This further proves the significance of orientation in regards to the East-West oriented distribution characteristics appear in the southern paleolake shore.

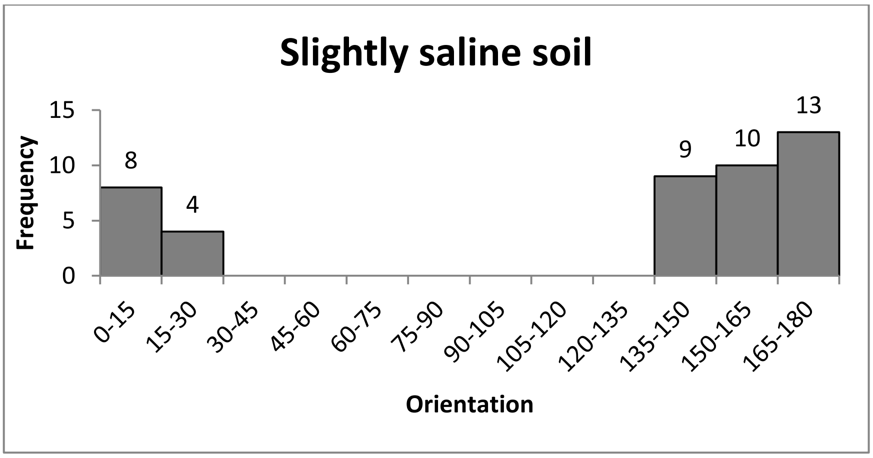

Figure 29 The orientation distribution of slightly saline soil (0-180 degree).

5.4.2 Feature Separability of Slightly Saline Soil

The extraction of slightly saline soil was based on orientation difference index, box length-to-width ratio and area ratio between polygon and minimum width bounding box. The Jeffries-Matusita distance (italic) and transformed divergence separability have been shown in Table 6 to test the separability of slightly saline soil (bold font) from other saline soils.

Table 6 The transformed divergence separability and Jeffries-Matusita distance (italic) of novel shape indices used for slightly saline soil feature extraction

Saline soil class	slightly saline soil	Moderately saline soil	Severely saline soil
Slightly saline soil	—	***1.7593***	***1.9857***
Moderately saline soil	**1.9361**	—	*1. 3408*
Severely saline soil	**2.0000**	1.4843	—

From Table 6, the slightly saline soil has very high transformed divergence separability (larger than 1.9). Specifically, the separability between slightly saline soil and severely saline soil has reached to 2 (perfect separable). These results prove the effectiveness of these three indices for separating slightly saline soil, although they have low separability between moderately saline soil and severely saline soil (1.4843, *1.3408*).

5.4.3 Basic Statistics of Moderately Saline Soil

From Table 7, the basic statistics of moderately saline soil have been summarised, including the area, perimeter, area ratio and perimeter ratio between polygon and box, orientation difference index, box length-to-width ratio as well as the box orientation. In comparison with Table 5 (slightly saline soils), the mean orientation difference index (ODI) (10.815) of moderately saline soil is far larger than that of (1.12) slightly saline soil. This further proves the effectiveness of ODI for characterizing the strong orientation and symmetric properties. The minimum width box length-to-width ratio of moderately saline soil (1.678 from Table 7) is far smaller than that of slightly saline soil (6.163 from Table 5). This statistical results show that the length-to-width ratio is extremely important for differentiating the slightly saline soil and moderately saline soil using geometric properties.

Table 7 The basic statistics (Minimum, Maximum, Mean and Stand Dev.) of novel shape indices for moderately saline soil

Moderately saline soil (117)	Area	Perimeter	PA/BA	PP/BP	ODI(°)	MWBL /MWBW	Orientation (°)
Minimum	17100	1078	0.209	0.831	0.027	1.045	0.718
Maximum	59722650	128033	0.51	3.768	74.434	2.789	179.305
Mean	5196586	22939	0.417	1.673	10.815	1.678	99.366
Stand Dev.	8964267	24352	0.064	0.503	11.45	0.445	51.747

The orientation histogram of moderately saline soil has been illustrated on Figure 30. It explicitly indicates the bimodal distribution of moderately saline soil. The peaks occur around 100 degree and 160 degree and mostly 100 degree, which is coincident with the mean of orientation (99.366). From literature and interviewing with the local citizens, the 100 degree orientation is highly related to the strong prevailing winds along Southwest to Northwest, mainly the lake groups of western Songnen Plain. The moderately saline soils around current lakes are far more uncertain and dynamic with bimodal distribution. Another peak of 160 degree is mainly because some of the lakes are approximate to circle without any directions, and in this circumstance, the orientation is mostly close to horizontal line (approaching to 0 or 180 degree).

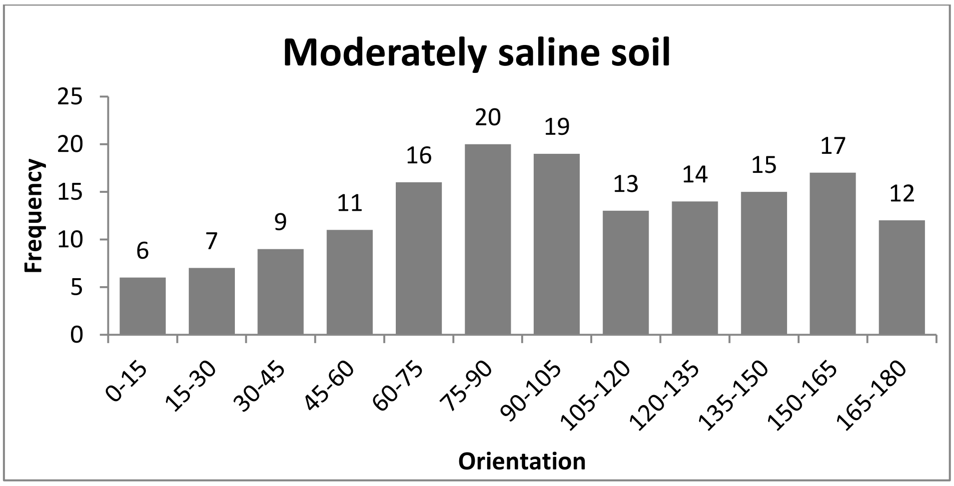

Figure 30 The orientation distribution of moderately saline soil (0-180 degree).

5.4.4 Feature Separability of Moderately Saline Soil

Similar to 5.4.2, the transformed divergence separability and Jeffries-Matusita distance (italic) of moderately saline soil have been shown in Table 8. The feature extraction of moderately saline soils around current lakes was based on minimum box length-to-width ratio, area ratio and perimeter ratio between polygon and box. The separability of moderately saline soils from slightly and severely saline soils (bold font) is very high (larger than 1.9) by using these three features. Notably, the separability of severely saline soil is also high with the introduction of perimeter ratio between polygon and box, which was utilized to differentiate the severely saline soil.

Table 8 The transformed divergence separability and Jeffries-Matusita distance (italic) of novel shape indices used for moderately saline soil feature extraction

Saline soil class	Slightly saline soil	Moderately saline soil	Severely saline soil
Slightly saline soil	—	***1.9316***	*1.7562*
Moderately saline soil	**1.9685**	—	***1. 9408***
Severely saline soil	1.8741	**1.9843**	—

5.4.5 Spatial Statistics of Severely Saline Soil

The feature extraction of severely saline soil is simple and straightforward based on size and geometric shape. The two features (polygon area and perimeter ratio between polygon and box) were used and the severely saline soils were effectively extracted. The transformed divergence separability and Jeffries-Matusita distance (italic) based on these two features are indicated in Table 9.

Table 9 The transformed divergence separability and Jeffries-Matusita distance (italic) of novel shape indices used for severely saline soil feature extraction

Saline soil class	Slightly saline soil	Moderately saline soil	Severely saline soil
Slightly saline soil	—	*0.8335*	***1.9441***
Moderately saline soil	1.3408	—	***1.9343***
Severely saline soil	**1.9961**	**2.0000**	—

The severely saline soil characterized by polygon area and ruggedness ratio has the perfect separability (around 2). And specifically, the severely saline soils have statistically significant different values of perimeter ratio between polygon and box because of complex and zigzag shapes.

5.4.6 Pair-wise Comparison between Representative Features

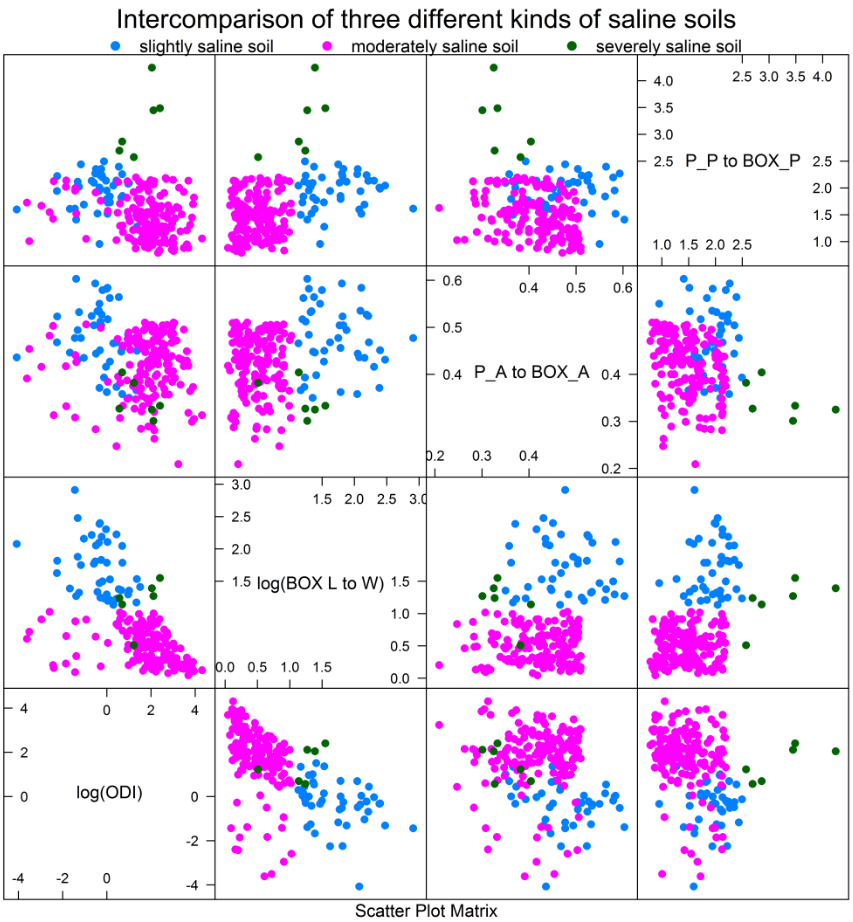

Figure 31 Scatter plot for inter-comparison of three different kinds of saline soils.

From Figure 31, the results of four representative indices (log of ODI, log of Box length-to-width, area ratio between polygon and box, perimeter ratio between polygon and box) have been pair-wisely compared using novel shape indices. The three kinds of saline soils with different geometric shape have been shown with different colours (blue, pink and green refer to slightly, moderately and severely saline soil respectively). The scatterplots further showed that the separability of orientation difference, box length-to-width and area ratio between polygon and box are high with seldom overlaps. The ruggedness (perimeter ratio between polygon and box) is completely separable for the severely saline soil from the other two types.

5.5 Saline Soil Pattern Analysis using Traditional Shape Indices

The traditional landscape pattern indices are used as a benchmark of our novel shape indices. The perimeter-area ratio, fractal dimension as well as traditional shape index have been tested for saline soil feature extraction using *Fragstat* 4.2.

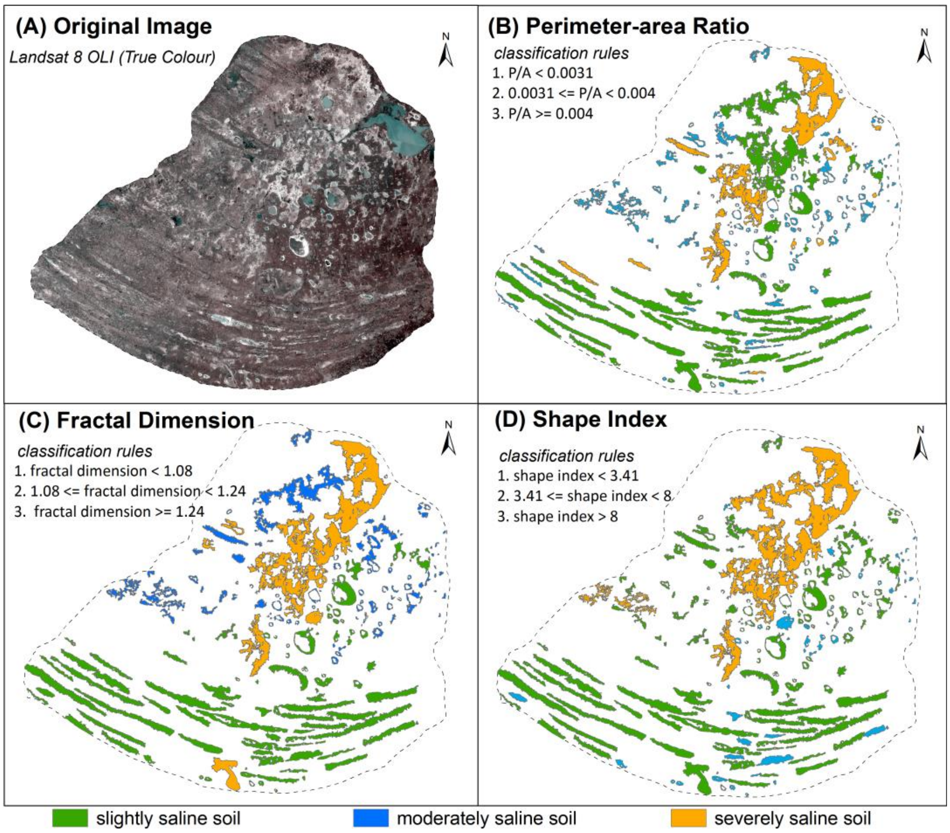

Figure 32 Saline soil classification results of (A) original Landsat 8 OIL true colour image based on traditional shape indices: (B) Perimeter-area Ratio, (C) Fractal Dimension and (D) Shape Index.

Figure 32 shows the results of traditional shape indices. The three indices (perimeter-area ratio, fractal dimension and shape index) all misclassify the slightly saline soil along large paleolake shore with some of the moderately saline soils around current lakes, especially the oxbow lake with distinctive curved shape. These two shapes have the similar perimeter-area ratio with strip-liked patterns but the slightly saline soils are more close to linear. Essentially, the fractal dimension and shape index are all based on the perimeter-area relationship without taking the effect of anisotropy into account. The perimeter-area ratio has also misclassified some severely saline soils while the fractal dimension and shape index can better differentiate them to some extent. The main reason is because of the size of the patch, which results in the variation of the traditional shape indices. For example, an increase in patch size will give rise to a decrease of perimeter-area ratio with the constant shape. The fractal dimension is purely based on the shape complexity (low, medium and high) instead of considering the shape orientation, angularity and compactness.

The transformed divergence separability and Jeffries-Matusita distance (italic) among three types of saline soils using three traditional indices have been tested and shown in Table 10. The separability between slightly saline soils and moderately saline soil is very low (1.2962). A relative high separability (1.8212) has achieved for the severely saline soils with the slightly saline soils, but still relatively low and tend to be confused with moderately saline soils.

Table 10 The transformed divergence separability and Jeffries-Matusita distance (italic) of the three traditional shape indices for saline soil feature extraction

Saline soil class	Slightly saline soil	Moderately saline soil	Severely saline soil
Slightly saline soil	—	*1.1129*	*1.7397*
Moderately saline soil	1.2962	—	*1.4886*
Severely saline soil	1.8212	1.617	—

5.6 Classification Accuracy Assessment

The validation sample plots (30 samples per class) were stratified randomly selected all over the study area from Landsat 8 OIL imagery. The centroids of sample plots were visually interpreted by Obview-3 Panchromatic imagery downloaded from USGS, Bing Map Aerial and Google Maps, and these validation sample plots were overlaid with reference maps provided by expert in paleogeography and soil scientists and further discussed with them to determine the degree of salinity. Table 11 shows the confusion matrices of the saline soil classification produced by the four methods: the perimeter-area ratio, fractal dimension, shape index and the proposed novel shape indices. The highest mapping accuracy of saline soil classification has been achieved with overall accuracy of 81.11% and Kappa of 0.72 by the proposed novel shape indices. However, the overall accuracies (kappa coefficient) of other three traditional landscape indices are low compared with the novel shape indices method, with 71.11% (kappa of 0.57) by perimeter-area ratio, 75.56% (kappa of 0.63) by fractal dimension and 74.44% (kappa of 0.62) by shape index. A Kappa z-test for pair-wise comparison proves that the accuracy derived from the proposed novel shape indices classification method is significantly higher than the accuracies produced by perimeter-area ratio, fractal dimension and shape index respectively (average z-value = 2.65, p = 0.008) (table 12).

Table 11 The producer's and user's accuracies of the saline soil classes achieved by the shape indices classifications in Western Songnen Plain; PA%- % producer's accuracy; UA %- % user's accuracy; OA –Overall Accuracy (%);kappa (Kappa Index Agreement/Kappa Coefficient); A – Slightly saline soil; B – Moderately saline soil; C – Severely saline soil.

	Perimeter-area ratio							Fractal Dimension					
	A	B	C	Total	PA (%)	UA (%)		A	B	C	Total	PA (%)	UA (%)
A	20	4	5	29	66.67	68.97	A	22	2	5	29	73.33	75.86
B	7	23	4	34	76.67	67.65	B	6	24	3	33	80.00	72.73
C	3	3	21	27	70.00	77.78	C	2	4	22	28	73.33	78.57
Total	30	30	30				Total	30	30	30			
					OA	71.11%						OA	75.56%
					Kappa	0.57						Kappa	0.63
	Shape index							Novel Shape Indices					
	A	B	C	Total	PA (%)	UA (%)		A	B	C	Total	PA (%)	UA (%)
A	22	5	3	30	73.33	73.33	A	25	1	2	28	83.33	89.29
B	5	22	4	31	73.33	70.97	B	3	26	5	34	86.67	76.47
C	3	3	23	29	76.67	79.31	C	2	3	23	28	76.67	82.14
Total	30	30	30				Total	30	30	30			
					OA	74.44%						OA	82.22%
					Kappa	0.62						Kappa	0.73

The individual average producer's and user's accuracy have been compared for each saline soil class classified by four methods. The classification accuracy of slightly saline soil is very high by the proposed novel shape indices method with 86.31% average mapping accuracy, higher than fractal dimension (74.60%), shape index (73.33%) and perimeter-area ratio (67.82%). Similarly, the mapping accuracy of moderately saline soil by the proposed method (81.57%) is much higher than the results of other three traditional landscape shape indices, with fractal dimension (76.37%) slightly higher than other two traditional indices (average 72.155%). The severely saline soil has a continuous tendency of increase for classification accuracy by the four methods, with the highest accuracy of 79.41% achieved by the proposed method.

Table 12 The kappa z-statistic of the proposed novel shape indices method compared with three traditional landscape indices with Kappa Z-test and corresponding p value. Significantly different accuracies with 95% confidence (z-value > 1.96) are indicated by *.

Saline soil classification	Kappa z-statistics (p-value)			
	Perimeter-area ratio	Fractal dimension	Shape index	Average
Proposed novel shape indices	3.07* (0.002)	2.36* (0.018)	2.51* (0.012)	2.65* (0.008)

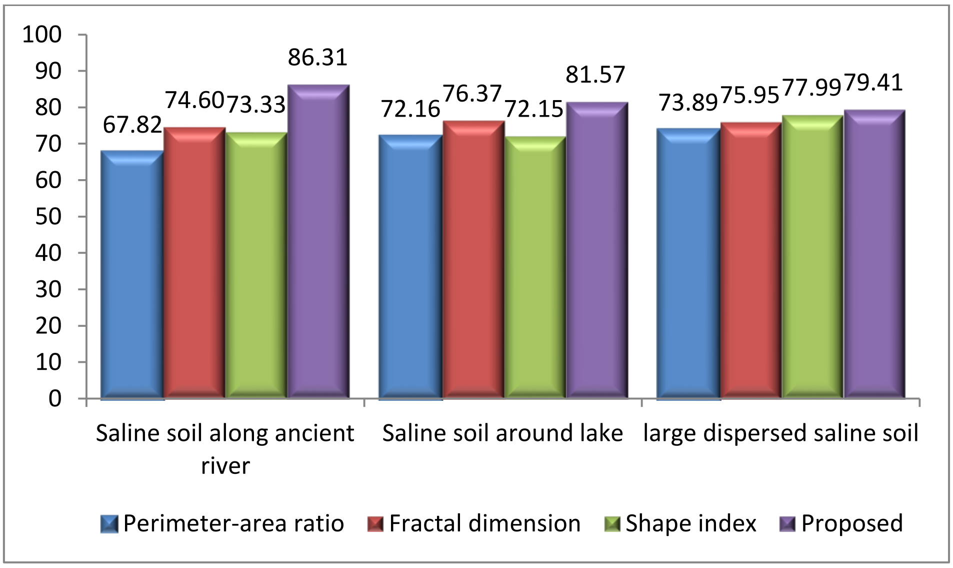

Figure 33 The comparison of mean producer's and user's accuracy (%) per class achieved by four classification methods in study area: Perimeter-area ratio, Fractal dimension, Shape index and the proposed novel shape indices

5.7 Linking Classification to Ecological Functions

The saline soil has been classified into three classes, i.e. slightly saline soil, moderately saline soil and severely saline soil. These three types of saline soils are different in terms of degree of salinity which might link to distinct ecological functions. According to existing literatures and local experts, these saline soils were sparsely covered by grass communities that are mostly salt tolerant species. The most distinguished difference lies in the vegetation growth ruined by these soils with different degree of salinity. The vegetation density is considered as an indicator, directly influenced by the distribution and degree of salt on the ground. The higher degree of salinity distributed, the lower density of vegetation exists. The Normalized difference vegetation index (NDVI), an effective index indicating the green vegetation growth, has been tested on the study area to prove the ecological meaning of saline soil classification. Basic statistics of three saline soils classes extracted by novel shape indices, including mean, median and standard deviation, have been summarized in Table 13. The NDVI values of slightly saline soils are the highest in comparison with other two classes with a mean of 0.3842 and a standard deviation (SD) of 0.1278. The moderately saline soils have the mean NDVI of 0.2816 and a standard deviation of 0.1367. However, the severely saline soils have the lowest mean NDVI value of 0.2364 and standard deviation of 0.1096. Pair-wised z-statistic test has shown that the NDVI differences between these three classes are significant (greater than 1.96) at 95% confidence level.

Table 13 NDVI Statistics of three saline soil classes with pair wised z-Test between each other. Significantly different accuracies with confidence of 95% (t-value > 1.96) are indicated by *.

Statistics		Slightly saline soil	Moderately saline soil	Severely saline soil
Mean		0.3842	0.2816	0.2364
Median		0.3854	0.2677	0.2258
Standard Deviation		0.1278	0.1367	0.1096
z-Test	Slightly saline soil	—		
	Moderately saline soil	15.4277*	—	
	Severely saline soil	25.0799*	8.7936*	—

The normal distribution curves of three classes have been plotted on Figure 34. Blue line represents the slightly saline soils with the largest mean NDVI value. The mean NDVI of green line (moderately saline soils) is larger than that of red line (severely saline soils), while the variances of these normal curves are significantly different. The moderately saline soil has higher degree of variation in NDVI value compared with the severely saline soil.

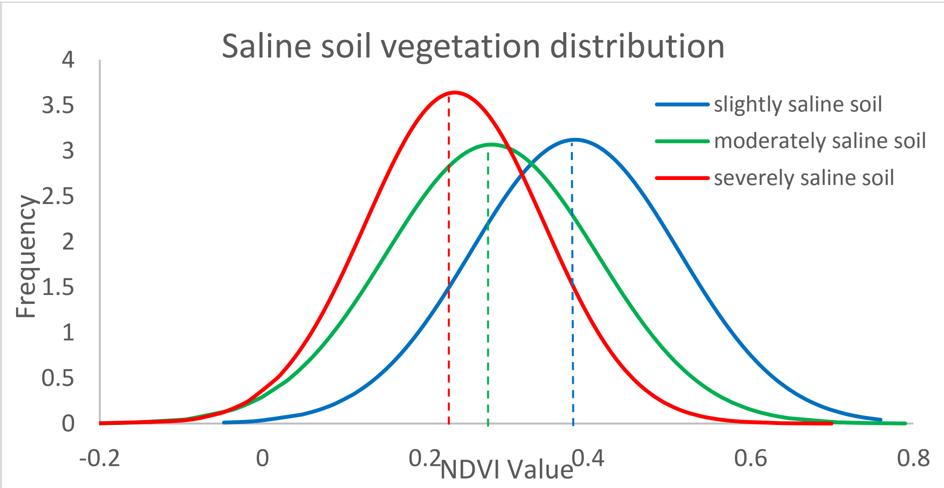

Figure 34 NDVI normal distribution curves of three saline soil classes. The dashed lines indicate the mean NDVIs of different classes

The results are conformed to the degree of salinity in the study area found by the expert in paleogeography and soil scientists. The slightly saline soil has the lowest level of salinity but highest vegetation density. The moderately saline soil has the medium level of salinity and a moderate vegetation density. However, the severely saline soil has the highest salinity level with the lowest vegetation density, which to a large extent lack of green vegetation and has no value on agricultural and grazing capability.

Table 14 summarizes the vegetation properties related to different saline soil classes and their corresponding degrees of soil salinity. The results were produced by overlaying the digital atlas of vegetation in China and the classification results and extract the dominant species. The different vegetation types dominant in different kinds of saline soils indicate the variation of ecological functions. The slightly saline soils along a large paleolake shore have slight to moderate degree of soil salinity and the dominant species of vegetation are *Leymus chinensis* and *Puccinellia tenuiflora*. The moderately saline soils around current lakes belong to the moderate soil salinity with dominant vegetation of *Puccinellia tenuiflora* and *Chloris virgata*. However, the severely saline soils are ecologically vulnerable with

high degree of soil salinity. Only those salt-tolerant species such as *Artemisia anthifolia* and *Suaeda corniculata* exist in these continuously distributed regions.
The soil physical characteristics of Western Songnen Plain have been summarized by Table 15 based on the field investigation by (Chi and Wang, 2010). Bulk density and saturated hydraulic conductivity were two field measurements illustrating the soil properties in regards to the different degree of soil salinity. The bulk density describes the soil particle size and the saturated hydraulic conductivity indicates the water permeability and infiltration. The bulk density rises along with the increasing degree of soil salinity. By contrast, the saturated hydraulic conductivity decreases with respect to the ascending soil salinity. These variations in soil physical properties further prove the difference in ecological functions and environmental conditions.

Table 14 A summary of vegetation characteristics related to different saline soil types and various degrees of soil salinity in the Western Songnen Plain, Northeast China

Saline soil types	Degree of soil salinity	Vegetation
Slightly saline soil	Slight to Moderate	*Leymus chinensis* *Puccinellia tenuiflora*
Moderately saline soil	Moderate	*Puccinellia tenuiflora* *Chloris virgata*
Severely saline soil	High	*Artemisia anthifolia* *Suaeda corniculata*

Table 15 A summary of soil physical characteristics related to different saline soil types and various degrees of soil salinity in the Western Songnen Plain, Northeast China (Chi and Wang, 2010)

Saline soil types	Degree of soil salinity	Bulk density ($g\ cm^{-3}$)	Saturated hydraulic conductivity (mm day^{-1})
Slightly saline soil	Slight to Moderate	1.33-1.50	0.85-3.42
Moderately saline soil	Moderate	1.43-1.57	0.03-0.24
Severely saline soil	High	1.44-1.62	0.02-0.22

By linking with the ecological functions, particularly with the vegetation and soil physical properties, the slightly, moderately and severely saline soils were found to be different in ecological meaning. The slightly saline soils along a large paleolake shore were possibly formed by alluvial fan with significant effect of micro-relief. The soil grain size is coarse and has high level of infiltration. Therefore, the degree of salinity is low in this type of saline soils. The majority of severely saline soils are located at the central region of the large paleolake with soil deposit plain land. The thick crust of salt-affected land was deposited by heavy clay. Such soil particle grain sizes are small with low capacity of infiltration. The soil salinity is mostly high in this kind of saline soil. Nevertheless, the moderately saline soils around current lakes have the degree of salinity in between other two types, i.e. slightly and severely saline soils. The micro-relief has certain amount of fluctuation and the soil particles have some infiltration effects. But the majority of moderately saline soils lie inside the large paleolake formed by lacustrine sediment deposits. The degree of salinity of moderately saline soil is slight to moderate in comparison with the slightly saline soils and severely saline soils.

6 Discussion

6.1 Significance of developing novel shape indices

Landscape pattern indices are quantitative approaches widely used in characterizing land-use/land-cover patterns and served as basic reference information for further landscape modelling and spatial statistics (Liu *et al.*, 2010). Landscape metrics at patch or segment level often incorporate shape indices to characterize patch size, shape, heterogeneities and boundary characteristics. For example, The shape index and fractal dimension as complexity indices have been used in predicting the plant species richness (Moser et al. 2002). Meanwhile, advances of new generation geo-information science and earth observation, especially the rapid progress of fine spatial resolution satellite remote sensing, brings new trends towards object-based, i.e. patch-based image analysis rather than purely manipulating on pixel statistical level in modern optical remote sensing. Such revolution further promotes the development of landscape pattern analysis, relevant to patch geometric shape indices in particular, to extract accurate and tangible information from the increasing amount of detailed geospatial data. For instance, Frohn (2006) applied square pixel metric (SqP) to distinguish image objects with similar spectral characteristics but different shape complexity. In essence, the purpose of shape indices is to accurately represent the real-world objects in terms of geometry. But in the face of geometric complexity and diversity of spatial patches (objects), traditional shape indices in geometric representation are not guaranteed in terms of uniqueness, consistency and completeness. Therefore, by introducing and combining the minimal width bounding box and the moment box, this research hopes to gain an insight on patch geometric characteristics. Based on these two bounding boxes (geometric invariables concerning to a polygon), novel landscape indices that is able to characterize patch spatial anisotropy and inner structures are further deduced.

6.2 Advantages of novel shape indices

Most patch shape metrics in landscape pattern analysis emphasize on geometric complexity and distinguish among patches and landscapes on the basis of overall complexity. Artificial and natural landscapes can be differentiated in most cases based on landscape shape complexity. The artificial landscapes are relatively low while the natural landscapes are relatively high in terms of shape complexity. Such metrics can to some extent measure the impact of natural and anthropogenic activities on landscape formation. However, the current shape complexity indices on the basis of perimeter-area relationships are dimensional indices. For example, suppose the equivalent area circle of a patch has the shape complexity P, in terms of the perimeter-area ratio, P is inversely proportional to the radius of circle. In other words, with the shape constant, an increase in patch size will cause a decrease in the current shape indices. Therefore, the characterized shape complexities are lack of 'uniqueness'. At the same time, the traditional shape indices cannot reflect the characteristics of anisotropy exist commonly in landscape patterns produced by directional geophysical phenomena (Zhang *et al.* 2006). Landscape pattern indices require deep investigation on their 'uniqueness' (scientific) and comprehensiveness in characterizing geometric shapes. Thereby, in this research, minimum width bounding box (MWBB) and moment box (MB) have been introduced, based on which novel shape indices for vector pattern analysis have been theoretically derived. The effectiveness of newly developed indices was verified by real geographical problems, i.e. to differentiate between elongated, circular and irregular features formed in different geographical and environmental conditions.

With respect to MWBB, it has been used to solve tolerance issues on silver polygons in GIS geometric intersections (Suri *et al.*, 1999; Cheung *et al.*, 2004; Kui Liu *et al.*, 2007; Sae-jung *et al.*, 2008), but never been introduced into landscape pattern analysis. Apart from special cases (seldom happens in reality) such as circle, square et al., the minimum width bounding box of a landscape patch is invariant in terms of translation, rotation and reflection. The length of MWBB determines the orientation, direction, compactness (area ratio between polygon and MWBB) and ruggedness (perimeter ratio between polygon and MWBB). These derived indices are constant value in geometric representation for characterizing the shape of a patch. The compactness and ruggedness reflect the shape complexity of patches related to spatial anisotropy. For instance, the slightly saline soils along large paleolake shore have strong anisotropic properties (growing along east-west paleolake shoreline directionally), and their compactness normally larger than moderately sail soils around current lakes. In addition, both compactness and ruggedness are dimensionless indices without being influenced by patch sizes. In regard to MB, the minimum bounding boxes was built upon moment major and minor axes of patches. Such box is also unique in general situation, and the orientation and vector orientation (direction) indices are fixed as well (Zhang *et al.* 2006).

For a spatial patch, the MWBB is fixed even if any inner structures and parts of polygon change, providing the range of minimum width bounding box remains constant. Nevertheless, the MB will alter along with the changing moment caused by inner structure variations. Therefore, the combination between MWBB and MB could reflect multiple structural properties and symmetric characteristics of patches. The orientation difference index (ODI), for instance, illustrates the oriented symmetric properties of landscape patches. The smaller ODI indicates the higher symmetric characteristics of patches. By contrast, the larger ODI represents the asymmetry of polygon with the shape of eccentrics. The experiments also proved that the slightly saline soil has high level of symmetry with small ODI values. Similarly, more geometric characteristics can be determined by mutual relationship between centroid and the central dividing line, such as left eccentric or right eccentric, et al. Due to the limited space of this dissertation, relevant research will be carried out in the future work.

The saline soil in western Songnen Plain, Northeast China includes elongating shaped slightly saline soil along a large paleolake shore (slight – moderate degree of soil salinity), entire round or moon shaped moderately saline soil around current lakes (moderate degree of soil salinity), severely saline soil at the central region of the large paleolake (high degree of soil salinity) and other saline soils (mostly small and isolated patches with variation in salinity level). The automatic recognition and classification of saline soil with various ecological formations, degrees of soil salinity and ecological functions, and the further construction of hierarchical saline soil spatial database are of significance to the scientific decision support in saline soil management, amelioration and utilization in the study area. However, different types of saline soil are extremely hard to differentiate and they often overlap in spectral space with confusions due to the extraordinary similar remotely sensed spectral signature and uncertainties. Moreover, the traditional shape complexity indices are difficult to distinguish slightly saline soil and moderately saline soil with similar shape complexity but obvious differences in spatial anisotropy. Thus, based on the rule sets developed by novel shape indices in this research, the saline soil has been successfully and accurately classified into different function levels with high overall accuracy and kappa coefficient compared with traditional landscape indices including perimeter-area ratio, fractal dimension and shape index. The transformed divergence separability and Jeffries-Matusita distance among different saline soil classes illustrate the novel shape indices are far more separable than traditional indices. Therefore, the proposed novel shape indices are effective in theory and promising in vector landscape pattern analysis and applications. It is worth to mention that the classification of saline soil is just a successful experiment of the new method. The real innovation of this research is successfully differentiating between elongated, circular and irregular features that are geographically clustering at specific locations. The correlations between different saline soil classes and geometric features or spatial locations are found by experts on field based on long term observation and reference maps. In other words, the novel shape indices are developed to classify saline soil features with different geometric shapes instead of predicting the degree of salinity. These novel shape indices are landscape quantitative approaches specifically applicable on characterising objects with orientation and symmetric properties. Therefore, such novel method, in the future, could be further applied on feature extraction of sand dune, landslide, invasive species, et al with specific orientation created by spatial anisotropy, such as wind, tectonic, pollination processes et al.

6.3 Limitations and future recommendations

This study proposed novel shape indices for vector landscape pattern analysis, and demonstrated its capability in the application of saline soil characterization and classification. Many aspects of the method have not been fully addressed yet, and further investigations are required. These limitations mainly related to the newly developed indices and their potential applications on saline soil classification.

6.3.1 Issues related to landscape shape indices

For those patches with relatively small size, their shape properties are hard to be characterized and quantified due to huge uncertainties of landscape geometric features. Both traditional shape indices and novel shape indices involve the challenge of landscape patches with diverse size and shape, and often lead to poor characterization in describing patches with small size. Therefore, the other saline soil (mainly small patches) has not been further distinguished in this study.

In addition, unlike traditional dimensional shape complexity indices, most of the proposed novel shape indices are dimensionless. The dimensionless indices are relatively invariant to the sizes with the same geometric shape. Such novel shape indices are suitable for pattern recognition and object-based remote sensing classification. However, in terms of land cover/use change and landscape dynamic, the sensitivity of novel shape indices might not be as high as traditional shape indices due to its robustness in geometric variations. Thus, the development of shape indices that are representative to both landscape characterization and dynamic requires further investigations.

Moreover, the scales issues commonly exist in ecological research have not been considered in this research. How to deal with complicated scale-dependent landscape remain challenges in landscape shape indices development. Therefore, future research should take consideration of multi-scale analysis e.g. using wavelet coefficient and wavelet analysis to explicitly indicate how scales influence the vector landscape characterization using the proposed novel shape indices.

6.3.2 Issues related to applications and saline soil classification

This study tested the novel shape indices and successfully demonstrated on an application of saline soil classification with practical values. However, the comprehensive and systematic analyses of various geometric features have not yet been completely done due to the actual distribution of study area and data volume restriction. Such comprehensive tests should be implemented based on theoretical and real landscapes. For example, the neutral landscape model, RULE, developed by (Gardner *et al.*, 1987) could be used to further clarify the practicability and applicability of these indices in quantifying landscape patterns.

Besides, rule-based classification has been carried out based on novel shape indices, which relies on the reproducible a priori knowledge to classify the desired geographic objects. This classification procedure is rapidly gained importance as it allows the image analysts to evaluate in a detailed and transparent way to understand the characteristics of the image objects by defining the threshold and class association (Xu, 2013; Belgiu *et al.*, 2014). However, building the classification rule sets is not a trivial task. Previous studies have developed classification rules based on human knowledge acquired by interviewing domain experts (Kohli *et al.*, 2012), by mimicking photo-interpreter knowledge (Lloyd *et al.*, 2002; Sebari and He, 2013), or by using expert knowledge gained through praxis (Myint *et al.*, 2011). In this research, the most relevant geometric features and corresponding thresholds have been defined by expert knowledge to classify the image objects. The feature selection and choice of threshold involve subjective and knowledge-based interpretations. Other data mining methods such as decision trees (Watanachaturaporn *et al.*, 2008), random forest (Rodriguez-Galiano *et al.*, 2012), et al. might select optimum and unbiased features, although some others find such approaches are empirically tuned to the analysed data and hardly to be transferable to other areas (Belgiu *et al.*, 2014).

In addition, the spatial resolution of Landsat 8 OIL images used in this research was 30 meters with a 15 meter panchromatic band. Such thematic resolution brought some uncertainties in object-based segmentation in some vague boundaries of saline soil, particularly the slightly saline soils are bounded by complex environment with mixed bare soil, grassland and cultivated land. Therefore, the OBIA spectral segmentation was conducted semi-automatically with some expert rectification. The segmentation itself is important and requires further researches. However, this was not the core issues dealt with in this study and the objects extracted were relatively sufficient to the consequent vector landscape pattern analysis based on geometric shape. Future works using high spatial resolution remote sensing images for OBIA by incorporating novel shape indices would provide more precise and detailed landscape pattern analysis in saline soil applications. The reference data for validation in this research were produced by digitalization of high spatial resolution images. Uncertainty involved in the reference data may contribute to problematic confusion matrices. Some studies about these issues can be found in literatures (Stein *et al.*, 2009; Foody, 2010). Therefore, it is necessary to conduct field survey and sampling in the future for precise classification validations.

Finally, primary analysis has been done to link the classification to ecological function by extracting NDVI values (Figure 34). It shows the difference in ecological vegetation distribution and their causal relationship between vegetation and soil salinity (Table 14). Nevertheless, much more deep researches should be done in the future for saline soil towards practical applications, e.g. linking novel shape indices to various geographical factors including local climate and hydrological conditions, micro relief et al. in order to further understand the formation and evolution of saline soil. The synthetic system integrating ground observation and remotely sensed data should be explored in the future research to quantitatively monitor the dynamics of saline soil.

7 Conclusions

In this research, novel shape indices were developed for vector landscape pattern analysis. The effectiveness was verified by real geographical problems in differentiating between elongated, circular and irregular features of different saline soil types. The indices based on minimum width bounding box and moment box could extract patch orientation, symmetry, compactness and ruggedness, and further classify the saline soil into ecological function level. Such novel indices were more accurate and robust for vector landscape quantitative analysis in comparison with traditional shape complexity indices including perimeter-area ratio, fractal dimension and shape index.

Firstly, two geometrically invariant bounding boxes, namely, the minimum width bounding box (MWBB) and moment box (MB), were newly introduced and successfully built up to represent patch orientation and geometric characteristics. The MWBB was firstly introduced to landscape pattern analysis by fitting the vector orientation and patch minimum width. Such vector oriented box can represent the general patch orientation and corresponding geometric shape characteristics. By contrast, the MB was built up based on centroid and moment of inertia, with moment orientation influenced by the inner structure and spatial distribution within patches. Both two boxes are theoretically derived to accurately represent the geometric orientation and shape characteristics.

Secondly, a series of indices have been successfully developed based on the two boxes, i.e. MWBB and MB, to reflect inner structure and shape complexity related to spatial anisotropy. The novel shape indices are geometric measurements of patch orientation and shape complexity, such as orientation, orientation difference between MB and MWBB, MWBB length-to-width ratio, perimeter-perimeter ratio, area-area ratio between polygon and MWBB etc. These novel indices are dimensionless metrics which are accurate and unique shape characterizations.

Thirdly, the effectiveness of the new landscape indices has been demonstrated by accurately identifying and distinguishing different saline soil types, i.e. slightly saline soil, moderately saline soil and severely saline soil. These saline soils are distinctively different in terms of geometric shape but similar in spectral characteristics. The spatial statistics, such as orientation histogram, transformed divergence separability, indicate that the novel shape indices are effective and separable by classification rule set development. The final classification results were superior to traditional shape indices, namely, the perimeter-area ratio, fractal dimension and shape index based on classification accuracy assessment.

Finally, by linking the classification results to ecological functions, distinct differences in vegetation and soil physical properties were found in slightly, moderately and severely saline soils differentiated by the proposed novel shape indices. The slightly saline soils are mostly located along a large paleolake shore within the study area, with coarse soil grain size and low degree of salinity. The vegetation density of such saline soil type is relatively high. In contrary, the severely saline soils are mainly continuously distributed at the central region of the large paleolake. The soil grain size is small with high degree of salinity and low occurrence of vegetation. Additionally, the moderately saline soils are geographically surrounding the current lakes with moderate vegetation and soil properties relative to the other two saline soil types.

In general, the novel shape indices have been developed and successfully demonstrated by differentiating spectrally similar saline soils with different geometric shape. The classification has significance in understanding and deriving the ecological functions and landscape formations. Therefore, it is concluded that the novel shape indices are promising approaches for vector landscape pattern analysis and ecological quantitative modelling.

References

Addink, E.A., Kleinhans, M.G. (2008) Recognizing meanders to reconstruct river dynamics of the Ganges. In *GEOBIA 2008 - Pixels, Objects, Intelligence: GEOgraphic Object Based Image Analysis for the 21st Century*.

Albrecht, J. (1999) Geospatial information standards. A comparative study of approaches in the standardisation of geospatial information. *Computers and Geosciences*. **25**(1), 9–24.

Anderson, D.C., Cychosz, J. (1990) An introduction to ray tracing. *Image and Vision Computing*. **8**(2), 169.

Ares, J., Bertiller, M., Del Valle, H. (2001) Functional and structural landscape indicators of intensification, resilience and resistance in agroecosystems in southern Argentina based on remotely sensed data. *Landscape Ecology*. **16**, 221–234.

Baatz, M., Schape, A. (2000) Multiresolution Segmentation : an optimization approach for high quality multi-scale image segmentation. *Journal of Photogrammetry and Remote Sensing*. **58**(3-4), 12–23.

Bailey, T.C., Gatrell, A.C. (1995) *Interactive spatial data analysis*.

Baker, W.L., Cai, Y. (1992) The r.le programs for multiscale analysis of landscape structure using the GRASS geographical information system. *Landscape Ecology*. **7**(4), 291–302.

Belgiu, M., Dr Guţ, L., Strobl, J. (2014) Quantitative evaluation of variations in rule-based classifications of land cover in urban neighbourhoods using WorldView-2 imagery. *ISPRS journal of photogrammetry and remote sensing : official publication of the International Society for Photogrammetry and Remote Sensing (ISPRS)*. **87**(100), 205–215.

Belongie, S., Belongie, S., Malik, J., Malik, J., Puzicha, J., Puzicha, J. (2002) Shape Matching and Object Recognition Using Shape Contexts. *IEEE Transactions on Pattern Analysis and Machine Intelligence*. **24**, 509–522.

Benz, U.C., Hofmann, P., Willhauck, G., Lingenfelder, I., Heynen, M. (2004) Multi-resolution, object-oriented fuzzy analysis of remote sensing data for GIS-ready information. *ISPRS Journal of Photogrammetry and Remote Sensing*. **58**(3-4), 239–258.

Blaschke, T. (2010) Object based image analysis for remote sensing. *ISPRS Journal of Photogrammetry and Remote Sensing*. **65**(1), 2–16.

Blaschke, T., Hay, G.J., Kelly, M., Lang, S., Hofmann, P., Addink, E., Queiroz Feitosa, R., van der Meer, F., van der Werff, H., van Coillie, F., Tiede, D. (2014) Geographic Object-Based Image Analysis - Towards a new paradigm. *ISPRS journal of photogrammetry and remote sensing : official publication of the International Society for Photogrammetry and Remote Sensing (ISPRS)*. **87**(100), 180–191.

Blaschke, T., Strobl, J. (2001) What’s wrong with pixels? Some recent developments interfacing remote sensing and GIS. *GIS*. **6**(6), 12–17.

Boles, S.H., Xiao, X., Liu, J., Zhang, Q., Munkhtuya, S., Chen, S., Ojima, D. (2004) Land cover characterization of Temperate East Asia using multi-temporal VEGETATION sensor data. *Remote Sensing of Environment*. **90**(4), 477–489.

Bruno, O.M., de Oliveira Plotze, R., Falvo, M., de Castro, M. (2008) Fractal dimension applied to plant identification. *Information Sciences*. **178**(12), 2722–2733.

Camastra, F., Vinciarelli, A. (2002) Estimating the intrinsic dimension of data with a fractal-based method. *IEEE Transactions on Pattern Analysis and Machine Intelligence*. **24**(10), 1404–1407.

Chan, C.K., Tan, S.T. (2001) Determination of the minimum bounding box of an arbitrary solid: An iterative approach. *Computers and Structures*. **79**(15), 1433–1449.

Chaudhuri, D., Samal, A. (2007) A simple method for fitting of bounding rectangle to closed regions. *Pattern Recognition*. **40**, 1981–1989.

Cheung, C.K., Shi, W., Zhou, X. (2004) A probability-based uncertainty model for point-in-polygon analysis in GIS. *GeoInformatica*. **8**(1), 71–98.

Chi, C.-M., Wang, Z.-C. (2010) Characterizing Salt-Affected Soils of Songnen Plain Using Saturated Paste and 1:5 Soil-to-Water Extraction Methods. *Arid Land Research and Management*. **24**(1), 1–11.

Chust, G., Ducrot, D., Pretus, J.L. (2004) Land cover mapping with patch-derived landscape indices. *Landscape and Urban Planning*. **69**, 437–449.

Cissel, J.H., Swanson, F.J., Weisberg, P.J. (1999) Landscape management using historical fire regimes: Blue River, Oregon. *Ecological Applications*. **9**, 1217–1231.

Csillag, F., Kabos, S. (2002) Wavelets, boundaries, and the spatial analysis of landscape pattern. *Ecoscience*. **9**, 177–190.

Dianwei, L., Zongming, W., Kaishan, S., Bai, Z., Liangjun, H., Ni, H., Sumei, Z., Ling, L., Chunhua, Z., Guangjia, J. (2009) Land use/cover changes and environmental consequences in Songnen Plain, Northeast China. *Chinese Geographical Science*. **19**(4), 299–305.

Drăguţ, L., Csillik, O., Eisank, C., Tiede, D. (2014) Automated parameterisation for multi-scale image segmentation on multiple layers. *ISPRS Journal of Photogrammetry and Remote Sensing*. **88**, 119–127.

Drăguţ, L., Tiede, D., Levick, S.R. (2010) ESP: a tool to estimate scale parameter for multiresolution image segmentation of remotely sensed data. *International Journal of Geographical Information Science*. **24**(6), 859–871.

Ecker, M.D., Gelfand, A.E. (1999) Bayesian modeling and inference for geometrically anisotropic spatial data. *Mathematical Geology*. **31**, 67–83.

Fan, C., Myint, S. (2014) A comparison of spatial autocorrelation indices and landscape metrics in measuring urban landscape fragmentation. *Landscape and Urban Planning*. **121**, 117–128.

Foody, G.M. (2010) Assessing the accuracy of land cover change with imperfect ground reference data. *Remote Sensing of Environment*. **114**(10), 2271–2285.

Forman, R.T.T. (1995) Some general principles of landscape and regional ecology. *Landscape Ecology*. **10**, 133–142.

Forman, R.T.T., Godron, M. (1986) Landscape Ecology. *Landscape Ecology*. **17**, 848.

Freeman, H., Shapira, R. (1975) Determining the minimum-area encasing rectangle for an arbitrary closed curve. *Communications of the ACM*. **18**, 409–413.

Fu, B., Chen, L. (2000) Agricultural landscape spatial pattern analysis in the semi-arid hill area of the Loess Plateau, China. *Journal of Arid Environments*. **44**, 291–303.

Gardner, R.H., Milne, B.T., Turnei, M.G., O'Neill, R. V. (1987) Neutral models for the analysis of broad-scale landscape pattern. *Landscape Ecology*. **1**(1), 19–28.

Girvetz, E.H., Greco, S.E. (2007) How to define a patch: A spatial model for hierarchically delineating organism-specific habitat patches. *Landscape Ecology*. **22**(8), 1131–1142.

Groom, G., Mücher, C.A., Ihse, M., Wrbka, T. (2006) Remote sensing in landscape ecology: Experiences and perspectives in a European context. In *Landscape Ecology*. pp. 391–408.

Gustafson, E.J. (1998) Minireview: Quantifying Landscape Spatial Pattern: What Is the State of the Art? *Ecosystems*. **1**(2), 143–156.

Hamazaki, T. (1996) Effects of patch shape on the number of organisms. *Landscape Ecology*. **11**(5), 299–306.

He, H.S., DeZonia, B.E., Mladenoff, D.J. (2000) An aggregation index (AI) to quantify spatial patterns of landscapes. *Landscape Ecology*. **15**(7), 591–601.

Helfenstein, J., Bauer, L., Clalüna, A., Bolliger, J., Kienast, F. (2014) Landscape ecology meets landscape science. *Landscape Ecology*. **29**, 1109–1113.

Honnay, O., Piessens, K., Van Landuyt, W., Hermy, M., Gulinck, H. (2003) Satellite based land use and landscape complexity indices as predictors for regional plant species diversity. *Landscape and Urban Planning*. **63**, 241–250.

Hu, J.F., Peng, P. a., Liu, M.Y., Xi, D.P., Song, J.Z., Wan, X.Q., Wang, C.S. (2015) Seawater Incursion Events in a Cretaceous Paleo-lake Revealed by Specific Marine Biological Markers. *nature*. **5**, 9508.

Huang, S., Siegert, F. (2006) Land cover classification optimized to detect areas at risk of desertification in North China based on SPOT VEGETATION imagery. *Journal of Arid Environments*. **67**(2), 308–327.

Hubbard, P.M. (1995) Collision detection for interactive graphics applications. *IEEE Transactions on Visualization and Computer Graphics*. **1**(3), 218–230.

Johnson, C.J., Boyce, M.S., Mulders, R., Gunn, A., Gau, R.J., Cluff, H.D., Case, R.L. (2005) Quantifying patch distribution at multiple spatial scales: Applications to wildlife-habitat models. *Landscape Ecology*. **19**(8), 869–882.

Kohli, D., Sliuzas, R., Kerle, N., Stein, A. (2012) An ontology of slums for image-based classification. *Computers, Environment and Urban Systems*. **36**(2), 154–163.

Kui Liu, Y., Qiang Wang, X., Zhe Bao, S., Gomboši, M., Žalik, B. (2007) An algorithm for polygon clipping, and for determining polygon intersections and unions. *Computers and Geosciences*. **33**(5), 589–598.

Kupfer, J.A. (2012) Landscape ecology and biogeography: Rethinking landscape metrics in a post-FRAGSTATS landscape. *Progress in Physical Geography*. **36**(3), 400–420.

Lambrechts, M.M., Caro, S., Charmantier, A., Gross, N., Galan, M.J., Perret, P., Cartan-Son, M., Dias, P.C., Blondel, J., Thomas, D.W. (2004) Habitat quality as a predictor of spatial variation in blue tit reproductive performance: A multi-plot analysis in a heterogeneous landscape. *Oecologia*. **141**(4), 555–561.

Lausch, A., Herzog, F. (2002) Applicability of landscape metrics for the monitoring of landscape change: Issues of scale, resolution and interpretability. In *Ecological Indicators*. pp. 3–15.

Leduc, A., Prairie, Y.T., Bergeron, Y. (1994) Fractal dimension estimates of a fragmented landscape: sources of variability. *Landscape Ecology*. **9**(4), 279–286.

Li, B.L. (2000) Fractal geometry applications in description and analysis of patch patterns and patch dynamics. *Ecological Modelling*. **132**, 33–50.

Li, B.L., Archer, S. (1997) Weighted mean patch size: A robust index for quantifying landscape structure. *Ecological Modelling*. **102**, 353–361.

Li, H., Wu, J. (2004) Use and misuse of landscape indices. *Landscape Ecology*. **19**(4), 389–399.

Li, X., He, H.S., Bu, R., Wen, Q., Chang, Y., Hu, Y., Li, Y. (2005) The adequacy of different landscape metrics for various landscape patterns. *Pattern Recognition*. **38**, 2626–2638.

Liu, J., Liu, M., Deng, X., Zhuang, D., Zhang, Z., Luo, D. (2002) The land use and land cover change database and its relative studies in China. *Journal of Geographical Sciences*. **12**(3), 275–282.

Liu, J.Y., Liu, M.L., Zhuang, D.F., Zhang, Z.X., Deng, X.Z. (2003) Study on spatial pattern of land-use change in China during 1995-2000. *Science in China Series D-Earth Sciences*. **46**(4), 373–384.

Liu, X., Li, X., Chen, Y., Tan, Z., Li, S., Ai, B. (2010) A new landscape index for quantifying urban expansion using multi-temporal remotely sensed data. *Landscape Ecology*. **25**(5), 671–682.

Llauss, A., Nogué, J. (2012) Indicators of landscape fragmentation: The case for combining ecological indices and the perceptive approach. *Ecological Indicators*. **15**, 85–91.

Lloyd, R., Hodgson, M.E., Stokes, A. (2002) Visual Categorization with Aerial Photographs. *Annals of the Association of American Geographers*. **92**(2), 241–266.

Mandelbrot, B.B. (1983) The Fractal Geometry of Nature. *American Journal of Physics*. **51**, 286.

Mathieu, R., Freeman, C., Aryal, J. (2007) Mapping private gardens in urban areas using object-oriented techniques and very high-resolution satellite imagery. *Landscape and Urban Planning*. **81**(3), 179–192.

McGarigal, K., Marks, B.J. (1995) *FRAGSTATS: Spatial Pattern Analysis Program for Quantifying Landscape Structure*.

Molina, A., Feito, F.R. (2002) A method for testing anisotropy and quantifying its direction in digital images. In *Computers and Graphics (Pergamon)*. pp. 771–784.

Moser, D., Zechmeister, H.G., Plutzar, C., Sauberer, N., Wrbka, T., Grabherr, G. (2002) Landscape patch shape complexity as an effective measure for plant species richness in rural landscapes. *Landscape Ecology*. **17**(7), 657–669.

Moskal, L.M., Styers, D.M., Halabisky, M. (2011) Monitoring urban tree cover using object-based image analysis and public domain remotely sensed data. *Remote Sensing*. **3**(10), 2243–2262.

Myint, S.W., Gober, P., Brazel, A., Grossman-Clarke, S., Weng, Q. (2011) Per-pixel vs. object-based classification of urban land cover extraction using high spatial resolution imagery. *Remote Sensing of Environment*. **115**(5), 1145–1161.

Neel, M.C., McGarigal, K., Cushman, S.A. (2004) Behavior of class-level landscape metrics across gradients of class aggregation and area. *Landscape Ecology*. **19**(4), 435–455.

O'Neill, R. V., Krummel, J.R., Gardner, R.H., Sugihara, G., Jackson, B., DeAngelis, D.L., Milne, B.T., Turner, M.G., Zygmunt, B., Christensen, S.W., Dale, V.H., Graham, R.L. (1988) Indices of landscape pattern. *Landscape Ecology*. **1**(3), 153–162.

O'Neill, R. V., Riitters, K.H., Wickham, J.D., Jones, K.B. (1999) Landscape pattern metrics and regional assessment. *Ecosystem Health*. **5**(4), 225–233.

Opdam, P., Verboom, J., Pouwels, R. (2003) Landscape cohesion: An index for the conservation potential of landscapes for biodiversity. *Landscape Ecology*. **18**, 113–126.

Pascual-Hortal, L., Saura, S. (2006) Comparison and development of new graph-based landscape connectivity indices: Towards the priorization of habitat patches and corridors for conservation. *Landscape Ecology*. **21**, 959–967.

Piasecki, R. (2000) Detecting self-similarity in surface microstructures. *Surface Science*. **454**(1), 1058–1062.

Pickett, S.T., Cadenasso, M.L. (1995) Landscape ecology: spatial heterogeneity in ecological systems. *Science*. **269**(5222), 331–334.

Puissant, A., Rougier, S., Stumpf, A. (2014) Object-oriented mapping of urban trees using Random Forest classifiers. *International Journal of Applied Earth Observation and Geoinformation*. **26**, 235–245.

Qiu, S., Wang, X., Zhang, S., Lian, Y., Zhang, Z., Zhu, J. (2012) The evolution of the large paleolake in Songliao Plain and its formation. *Quaternary Sciences*. **32**(5), 1011 –1021.

Ran, Y.H., Li, X., Lu, L., Li, Z.Y. (2012) Large-scale land cover mapping with the integration of multi-source information based on the Dempster–Shafer theory. *International Journal of Geographical Information Science*. **26**(1), 169–191.

Rizkalla, C.E., Moore, J.E., Swihart, R.K. (2009) Modeling patch occupancy: Relative performance of ecologically scaled landscape indices. *Landscape Ecology*. **24**, 77–88.

Rodriguez-Galiano, V.F., Ghimire, B., Rogan, J., Chica-Olmo, M., Rigol-Sanchez, J.P. (2012) An assessment of the effectiveness of a random forest classifier for land-cover classification. *ISPRS Journal of Photogrammetry and Remote Sensing*. **67**(1), 93–104.

Sae-jung, J., Chen, X.Y., Phuong, D.M. (2008) ERROR PROPAGATION MODELING IN GIS POLYGON OVERLAY. *Remote Sensing and Spatial Information Sciences*. **37**, 825–836.

Saha, B.N., Ray, N., Greiner, R., Murtha, A., Zhang, H. (2012) Quick detection of brain tumors and edemas: A bounding box method using symmetry. *Computerized Medical Imaging and Graphics*. **36**, 95–107.

Saura, S., Pascual-Hortal, L. (2007) A new habitat availability index to integrate connectivity in landscape conservation planning: Comparison with existing indices and application to a case study. *Landscape and Urban Planning*. **83**, 91–103.

Schönfisch, B. (1997) Anisotropy in cellular automata. *BioSystems*. **41**, 29–41.

Sebari, I., He, D.C. (2013) Automatic fuzzy object-based analysis of VHSR images for urban objects extraction. *ISPRS Journal of Photogrammetry and Remote Sensing*. **79**, 171–184.

Shen, G. (2002) Fractal dimension and fractal growth of urbanized areas. *International Journal of Geographical Information Science*. **16**(5), 419–437.

Stein, A., Hamm, N.A.S., Ye, Q. (2009) Handling uncertainties in image mining for remote sensing studies. *International Journal of Remote Sensing*. **30**(20), 5365–5382.

Suri, S., Hubbard, P.M., Hughes, J.F. (1999) Analyzing bounding boxes for object intersection. *ACM Transactions on Graphics*. **18**(3), 257–277.

Szegedy, C., Toshev, a, Erhan, D. (2013) Deep Neural Networks for Object Detection. *Advances in Neural Information …*, 1–9.

Tandeo, P., Autret, E., Chapron, B., Fablet, R., Garello, R. (2014) SST spatial anisotropic covariances from METOP-AVHRR data. *Remote Sensing of Environment*. **141**, 144–148.

Tanner, J.E. (2003) Patch shape and orientation influences on seagrass epifauna are mediated by dispersal abilities. *Oikos*. **100**(3), 517–524.

Toussaint, G. (1983) Solving geometric problems with the rotating calipers. In *IEEE MELECON83*. pp. 1–8.

Turner, M.G. (2005) Landscape ecology in North America: Past, present, and future. *Ecology*. **86**(8), 1967–1974.

Turner, M.G. (1989) Landscape Ecology: The Effect of Pattern on Process. *Annual Review of Ecology and Systematics*. **20**, 171–197.

Turner, M.G. (2005) LANDSCAPE ECOLOGY: What Is the State of the Science? *Annual Review of Ecology, Evolution, and Systematics*. **36**, 319–344.

Turner, M.G. (1990) Spatial and temporal analysis of landscape patterns. *Landscape Ecology*. **4**(1), 21–30.

Uuemaa, E., Antrop, M., Marja, R., Roosaare, J., Mander, Ü. (2009) Landscape Metrics and Indices : An Overview of Their Use in Landscape Research Imprint / Terms of Use. *Living Reviews in Landscape Research*. **3**, 1–28.

Vermote, E.F., Tanré, D., Deuzé, J.L., Herman, M., Morcrette, J.J. (1997) Second simulation of the satellite signal in the solar spectrum, 6s: an overview. *IEEE Transactions on Geoscience and Remote Sensing*. **35**(3), 675–686.

Vieira, M.A., Formaggio, A.R., Rennó, C.D., Atzberger, C., Aguiar, D.A., Mello, M.P. (2012) Object Based Image Analysis and Data Mining applied to a remotely sensed Landsat time-series to map sugarcane over large areas. *Remote Sensing of Environment*. **123**, 553–562.

Waller, L.A., Gotway, C.A. (2004) *Applied Spatial Statistics for Public Health Data*.

Wang, L., Seki, K., Miyazaki, T., Ishihama, Y. (2009) The causes of soil alkalinization in the Songnen Plain of Northeast China. *Paddy and Water Environment*. **7**(3), 259–270.

Watanachaturaporn, P., Arora, M.K., Varshney, P.K. (2008) Multisource classification using support vector machines: An empirical comparison with decision tree and neural network classifiers. *Photogrammetric Engineering and Remote Sensing*. **74**(2), 239–246.

Van der Werff, H.M.A., van der Meer, F.D. (2008) Shape-based classification of spectrally identical objects. *ISPRS Journal of Photogrammetry and Remote Sensing*. **63**(2), 251–258.

Werman, M., Keren, D. (2001) A Bayesian Method for Fitting Parametric and Nonparametric Models to Noisy Data. *TRANSACTIONS ON PATTERN ANALYSIS AND MACHINE INTELLIGENCE*. **23**, 528–534.

Woodcock, C.E., Strahler, A.H. (1987) The factor of scale in remote sensing. . **332**, 311–332.

Wu, J. (2004) Effects of changing scale on landscape pattern analysis: Scaling relations. *Landscape Ecology*. **19**(2), 125–138.

Wu, J., Hobbs, R. (2007) Landscape ecology : the state-of-the-science. In *Key topics in landscape ecology*. pp. 271–287.

Wu, J., Jelinski, D.E., Luck, M., Tueller, P.T. (2000) Multiscale Analysis of Landscape Heterogeneity: Scale Variance and Pattern Metrics. *Annals of GIS*. **6**(1), 6–19.

Xian, G., Homer, C., Fry, J. (2009) Updating the 2001 National Land Cover Database land cover classification to 2006 by using Landsat imagery change detection methods. *Remote Sensing of Environment*. **113**(6), 1133–1147.

Xu, H.Q. (2013) Rule-based impervious surface mapping using high spatial resolution imagery. *International Journal of Remote Sensing*. **34**(1), 27–44.

Ye, X., Wang, T., Skidmore, A.K. (2013) Spatial pattern of habitat quality modulates population persistence in fragmented landscapes. *Ecological Research*. **28**(6), 949–958.

Zhang, D., Shijie, W. (2001) Mechanism of freeze-thaw action in the process of soil salinization in northeast China. *Environmental Geology*. **41**(1-2), 96–100.

Zhang, S., Zhang, J., Li, F., Cropp, R. (2006) Vector analysis theory on landscape pattern (VATLP). *Ecological Modelling*. **193**, 492–502.

Zhu, Q., Gong, J., Zhang, Y. (2007) An efficient 3D R-tree spatial index method for virtual geographic environments. *ISPRS Journal of Photogrammetry and Remote Sensing*. **62**(3), 217–224.